CHAPTER THREE

SPREAD SPECTRUM MODULATION TECHNIQUES

SS technologies have been incorporated in numerous fields over recent years. In the military environment, Frequency Hopped Spread Spectrum (FH-SS) has been used extensively for robustness against jamming, while in telecommunications, such as power line communications and wireless services (voice and data), DS-SS has also been used extensively. To elaborate on the field of wireless cellular networks, the ITU established a suite of standards, collectively called IMT-2000. This standard is the driving force of the developments for the enhanced 3G standards in order to supply the current and future needs of wireless services. Particularly the 3GPP and 3GPP2 are developing the UMTS technologies and cdma2000 respectively, which in fact are based upon SS systems. One of the main challenges in the 3G evolution is the improvement of the downlink capacity, and for this reason one of the development directions moved to SS systems.

Further advantages provided by SS systems are, amongst others:

- Increased user capacity
- Ability of interfering signal rejection
- Multiple Access Interference (MAI) rejection capability
- Resistance to multipath fading

Modulation and demodulation techniques strive to achieve greater power and/or bandwidth efficiency in wireless channels. Since bandwidth is a limited resource, one of the primary design objectives of most modulation schemes is to minimize the required transmission bandwidth. SS techniques, on the other hand, employ a transmission bandwidth that is several orders of magnitude greater than the minimum required signal bandwidth. While this system is very bandwidth inefficient for a single user, the advantage of SS is that many users can simultaneously use the same bandwidth without significantly interfering with one another. Besides the power control problems experienced with SS systems, and the substantial prize paid in receiver complexity and processing power, SS systems become bandwidth efficient in a multiple-user environment.

Apart from occupying a very large bandwidth, SS signals are pseudorandom and have noise-like properties when compared with the digital information data. The spreading waveform is controlled by a spreading sequence or spreading code, which is a sequence that appears to be random, but can be reproduced in a deterministic manner by intended receivers. SS signals are demodulated at the receiver through cross-correlation with a locally generated version of the pseudorandom carrier. Cross-correlation with the correct spreading sequence despreads the SS signal and restores the modulated message in the same narrow-band as the original data, whereas cross-correlating the signal from an undesired user results in MAI at the receiver output.

SS modulation has many properties that make it particularly well suited for use in the mobile radio environment. The most important advantage is its inherent interference rejection capability. In the case of DSSS each user is assigned a unique spreading code which is approximately orthogonal to the codes of other users. The receiver can separate each user, based on their codes, even though they occupy the same spectrum at all times (note that this is

not the case with FH-SS). This implies that, up to a certain number of users, interference between SS signals using the same frequency is negligible. A general rule of thumb is that approximately 10% of the available spreading sequence family may be used before excessive MAI will occur, resulting in rapid receiver performance degradation. Not only can a particular SS signal be recovered from a number of other SS signals, it is also possible to recover information from a SS signal even when a narrowband interferer jams it. Since narrowband interference affects only a small portion of the SS signal, it can easily be removed through notch filtering without much loss of information [6].

Resistance to multipath fading [1, 6, 7] is another fundamental reason for considering SS systems for wireless communications, and in particular, this dissertation. It is known that wideband signals are frequency selective. Since the transmitted SS signals have uniform energy over a very large bandwidth, theoretically, only a small portion of the spectrum will undergo fading at any given time. Viewed in the time domain, the multipath resistance properties are due to the fact that the delayed versions of the transmitted spreading code sequence will have poor correlation with the original spreading code sequence, and will thus appear as another uncorrelated user, which is suppressed by the receiver. That is, as long as the multipath channel induces at least one chip delay, the multipath signals will arrive at the receiver such that they are shifted in time by at least one chip from the intended signal. The correlation properties of spreading code sequences are such that this slight delay causes the multipath to appear uncorrelated with the intended signal, so that the multipath contributions appear invisible to the desired received signal. SS systems are not only resistant to multipath fading, but they can also exploit the delayed multipath components to improve the performance of the system. This can be done by using a RAKE receiver that anticipates multipath propagation delays of the transmitted SS signal and combines the information obtained from several resolvable multipath components to form a stronger version of the signal. A RAKE receiver consists of a bank of correlators, each of which correlates with a particular multipath component of the desired signal. The correlator outputs may be weighted according to their relative strengths and summed, using maximum ratio receive combining methods to obtain the final signal estimate. For in depth discussions on RAKE receivers, see [6, 11].

This chapter is structured as follows: In *Section 3.1* a general overview of PN sequences is presented, followed with CSSs in *Section 3.2 and* Walsh Sequences in *Section 3.3*. In *Section 3.4* DS-SS theory is presented, followed with DS-SS probability of error theory in S*ection 3.5*. Space-Time Spreading (STS) theory is presented in *Section 3.6*, and lastly, the focus of *Section 3.7* is a literature study of ST coding, combined with CDMA technology.

3.1 SPREADING SEQUENCES

With SS modulation techniques, spreading codes are used to expand the bandwidth of the transmitted signal. The following are some of the different types of spreading codes commonly used:

- PN sequences
- Gold- and Kasami sequences
- Walsh sequences
- Complex Spreading sequences (CSS)

A PN or pseudorandom sequence is a binary sequence with an autocorrelation that resembles, over a period, the autocorrelation of a random binary sequence. Its autocorrelation also roughly resembles the autocorrelation of bandlimited white noise. Although it is deterministic, a PN sequence has many characteristics that are similar to those of random binary sequences, such as having a nearly equal number of zeros and ones, very low correlation between shifted versions of the sequence, very low cross-correlation between any two sequences, etc. PN sequences of length $N = 2^m-1$, generated by a linear feedback register of length m, are generally known as maximal length or m-sequences. PN sequences with improved periodic cross-correlation properties over maximal length sequences have been defined by Gold [54]. These codes are the well known Gold-sequences.

Walsh spreading codes are designed such that they do not interfere with each other in an ideal real life environment and are generally designed using the Hadamard matrix (an in depth discussion on the Hadamard matrix is presented in *Section 3.3*). However, orthogonality between the codes requires the codes to be time synchronized, i.e. they are only perfectly

orthogonal at zero relative time shifts and requires perfect chip synchronisation. Therefore orthogonal spreading codes are only used in the downlink of cellular 2.5G and beyond cellular systems. An example of an orthogonal spreading code is the Walsh-derived Orthogonal Variable Spreading Factor (OVSF) codes [11] used in the 3GPP and 3GPP2 standards.

Since the introduction of SS, binary spreading sequences have exhaustively been researched with DS-SS applications. Interest recently started to shift towards using non-binary and CSSs because of potential larger sets of sequences and improved cross-correlation properties compared to binary spreading sequences. Two mayor advantages of using CSSs in future 4G cellular systems are the possibility to transmit Constant Envelope (CE) and even Single Sideband (SSB) [55, 56] transmitter output signals. See *Section 3.2* for details regarding the CSSs used in this dissertation.

3.2 COMPLEX SPREADING SEQUENCES

This section briefly describes the filtered and un-filtered CSS families considered in this study.

3.2.1 Unfiltered Sequences

Zadoff-Chu Sequences

Zadoff-Chu (ZC) CSSs is a subclass of General Chirp-like (GCL) CSSs [57], which is generated and characterised as follows: Let $\bar{S}_{ZC}^{q} = \left\{S_{ZC}^{q}[0], S_{ZC}^{q}[1], \cdots, S_{ZC}^{q}[M_{seq}-1]\right\}$ represent the vector of chips of the q^{th} length-M_{seq} unfiltered continuous-time ZC sequence $S_{ZC}^{q}(t)$. With $j=\sqrt{-1}$, the i^{th} chip in this sequence is determined as follows [59], [60]:

$$S_{ZC}^{q}[i] = \begin{cases} \exp\left(j\dfrac{\pi \cdot a \cdot i^{2}}{M_{seq}}\right) & \text{if } M_{seq} \text{ is even} \\ \exp\left(j\dfrac{\pi \cdot a \cdot i(i+1)}{M_{seq}}\right) & \text{if } M_{seq} \text{ is odd} \end{cases} \tag{3.1}$$

where the sequence number a can only take on integer values relatively prime to M_{seq}. As such, the family size for length-M_{seq} ZC CSSs is calculated as follows:

$$M_{fam} = 1 + \sum_{a=2}^{M_{seq}-1} \begin{cases} 1 & if\ M_{seq} \bmod(a) \neq 0 \\ 0 & if\ M_{seq} \bmod(a) = 0 \end{cases} \tag{3.2}$$

Hence, the largest ZC CSS families are obtained when M_{seq} is an odd prime number. In such a case the family size is $M_{fam} = M_{seq}$ -1 [60].

Quadriphase Sequences

Quadriphase (QPH) sequences are closely related to binary sequences. A length- M_{seq} QPH sequence's chip vector $\bar{S}^q_{QPH} = \left\{S^q_{QPH}[0], S^q_{QPH}[1], \cdots, S^q_{QPH}[M_{seq}-1]\right\}$ is constructed using two length-M_{seq} binary sequences' chip vectors, denoted as $\bar{S}^q_A = \left\{S^q_A[0], S^q_A[1], \cdots, S^q_A[M_{seq}-1]\right\}$ and $\bar{S}^q_B = \left\{S^q_B[0], S^q_B[1], \cdots, S^q_B[M_{seq}-1]\right\}$, respectively. Calculation of the i^{th} chip of the QPH sequence is accomplished as follows [60]:

$$S^q_{QPH}[i] = \frac{1}{2\sqrt{2}}(1+j)S^q_A[i] + \frac{1}{2\sqrt{2}}(1-j)S^q_B[i] \tag{3.3}$$

It follows that each chip in the QPH sequence will have a value from the complex 4-symbol alphabet $\left\{\frac{1}{\sqrt{2}}+\frac{j}{\sqrt{2}}, \frac{1}{\sqrt{2}}-\frac{j}{\sqrt{2}}, -\frac{1}{\sqrt{2}}+\frac{j}{\sqrt{2}}, -\frac{1}{\sqrt{2}}-\frac{j}{\sqrt{2}}\right\}$, if the binary sequences' chip vectors $\bar{S}^q_A$ and $\bar{S}^q_B$ have chips from the antipodal alphabet $\{-1;1\}$. For *Alltop*-type QPH sequences [60], the family size is given as $M_{fam} = M_{seq}$ - 1, with the sequence length M_{seq} limited to prime values. Furthermore, using Gold binary sequences for $\bar{S}^q_A$ and $\bar{S}^q_B$ is a popular approach [61]. Since QPH sequences are binary in nature, it follows that their complex envelopes will not be constant.

3.2.2 Filtered Sequences

DSB CE-LI-RU Filtered GCL Sequences

It has been shown that ZC sequences contain all the frequencies in the range [0;M_{fam} / T_{chip}) [Hz], with T_{chip} the duration of a chip [61]. Thus, the bandwidth of such sequences are a function of the family size. In order to bandlimit $S_{ZC}^{q}(t)$ and remove its dependency on the sequence index a, a mod(2π) phase constraint can be incorporated, resulting in a *Chu* sequence's chip vector denoted as $\bar{S}_{Chu}^{q} = \left\{S_{Chu}^{q}[0], S_{Chu}^{q}[1], \cdots, S_{Chu}^{q}[M_{seq}-1]\right\}$ [59], [60]. The i^{th} chip of a *Chu* sequence is determined as follows:

$$S_{Chu}^{q}[i] = \begin{cases} \exp\left(j\dfrac{\pi \cdot a \cdot i^{2}}{M_{seq}}\right)\bmod(2\pi) & \text{if } M_{seq} \text{ is even} \\ \exp\left(j\dfrac{\pi \cdot a \cdot i(i+1)}{M_{seq}}\right)\bmod(2\pi) & \text{if } M_{seq} \text{ is odd} \end{cases} \tag{3.4}$$

It has been shown [60] that the bandwidth of *Chu* sequences are 1/T_{chip} [Hz]. Double Side Band Constant Envelope Linearly Interpolated Root-of-Unity (DSB CE-LI-RU) filtered GCL sequences are obtained by filtering $S_{Chu}^{q}[i]$ with a *linearly interpolating root-of-unity filter* [62] in order to achieve the minimum Nyquist bandwidth of 1/(2.T_{chip}) [Hz]. The family size of such sequences is also given by *Equation (3.2)*. Furthermore, these sequences exhibit constant complex envelopes.

ABC Sequences

Analytic Bandlimited Complex (ABC) sequences are generated by appropriately modifying the previously defined DSB CE-LIRU filtered GCL sequences in order to produce an injective function, as described in [56]. When used in balanced QPSK structures, ABC sequences [56] exhibit analytical properties, i.e. a SSB DS/SSMA signal is obtained after modulation onto the in-phase and quadrature carriers [60]. As with ZC and DSB CE-LI-RU filtered GCL sequences, the family size of ABC CSSs is determined using *Equation (3.2)*.

3.3 WALSH SEQUENCES

Walsh spreading codes are obtained from Hadamard matrices. A Hadamard matrix M_j is a j x j matrix (j is an even integer) of 1s and 0s with the property that any row differs from any other row in exactly $\frac{1}{2}j$ positions. One row of the matrix contains al zeros and the other rows contain $\frac{1}{2}j$ ones and $\frac{1}{2}j$ zeros. For j = 2, the Hadamard matrix is

$$M_2 = \begin{bmatrix} 0 & 0 \\ 0 & 1 \end{bmatrix} \tag{3.5}$$

Furthermore, from M_j, a Hadamard matrix of M_{2j} can be generated according to the relation

$$M_{2j} = \begin{bmatrix} M_j & M_j \\ M_j & \overline{M}_j \end{bmatrix} \tag{3.6}$$

where $\overline{M}_j$ denotes the complement (0s replaced by 1s and vice versa) of M_j. Thus, by substituting *Equation (3.5)* into *Equation (3.6)*, *Equation (3.7)* is obtained.

$$M_4 = \begin{bmatrix} 0 & 0 & 0 & 0 \\ 0 & 1 & 0 & 1 \\ 0 & 0 & 1 & 1 \\ 0 & 1 & 1 & 0 \end{bmatrix} \tag{3.7}$$

By the repeated application of *Equation (3.6)*, Hadamard matrix's with block length of $\varsigma = 2^i$ can be generated, where i is a positive integer. Once a Hadamard matrix is constructed, a Walsh code is obtained by selecting, as code words, the rows of a Hadamard matrix and the number of columns in the Hadamard matrix determines the length of the Walsh spreading code. For example, 2 Walsh spreading codes of length, ς = 4 from *Equation (3.7)* is

$$Code1 = 0\,1\,0\,1 \tag{3.8}$$

$$Code2 = 0\,0\,1\,1 \tag{3.9}$$

3.3.1 Correlation properties

The major tasks of any spreading code used in wireless communications systems are the following:

- Spreading the bandwidth of the modulated signal to a larger bandwidth, and
- to distinguish between the spreading sequences of different users' signals that utilise the same transmission bandwidth in a multiple-access scheme.

To meet these requirements, the sequences need special correlation properties, i.e. periodic auto-correlation, and periodic cross-correlation. Periodic autocorrelation, $R_a(\tau)$, in general, is defined by the integral

$$R_a(\tau) = \int_{-\infty}^{\infty} f(t) \cdot f(t-\tau) dt \qquad (3.10)$$

It is a measure of the similarity between a signal $f(t)$ and a τ-second time shifted replica of itself. In other words, the auto-correlation function is a plot of all time shifts τ, of $f(t-\tau)$ correlated with itself and is mostly used for synchronization purposes (see *Figure 3.1*).

From *Figure 3.1* it is evident that the periodic auto-correlation properties of Walsh sequences are not satisfactory. The multiple auto-correlation peaks over one sequence length, *N*, observed in *Figure 3.1* will lead to synchronisation ambiguities in the receiver. A satisfactory result would have been one single spike in time and the rest of the periodic autocorrelation function zero. In the case of the DSSTS scheme presented in *Chapter 5*, perfect synchronization is assumed and the simulations are not performed in a multipath environment, making the periodic auto-correlation unimportant. Thus, no echoes are received at the receiver and the auto-correlation is for this reason not a critical design factor. However, in the case of the SSTD scheme presented in *Chapter 5*, a multipath flat fading channel was considered and for this reason, Walsh spreading codes were not used in the SSTD scheme.

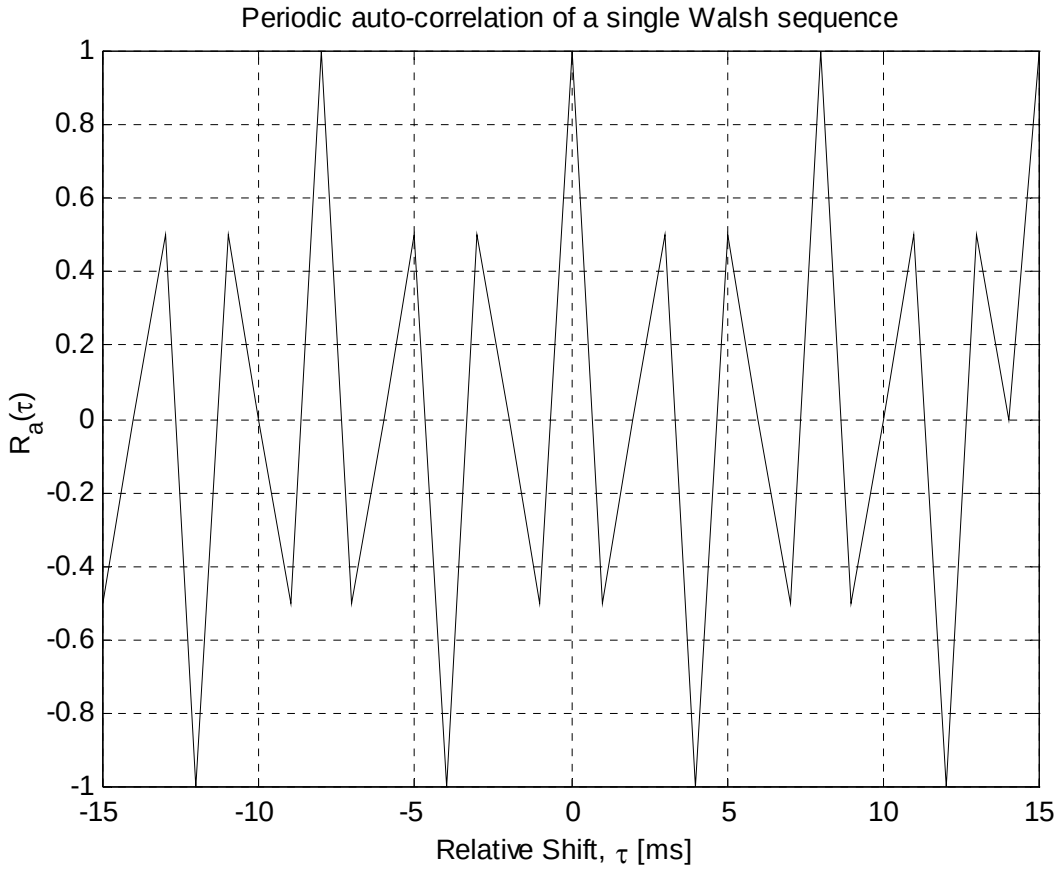

Figure 3.1. Periodic auto-correlation of a length *N* = 16 Walsh sequence taking one sample per chip.

The periodic cross-correlation between different antennas is rather an important design factor in both the DSSTS scheme as well as the SSTD scheme, because of the multi-antenna scenario. Periodic cross-correlation $R_c(\tau)$, is defined as the correlation of two different signals $f(t)$ and $g(t)$, and is defined as

$$R_c(\tau) = \int_{-\infty}^{\infty} f(t) \cdot g(t-\tau) dt \qquad (3.11)$$

The periodic cross-correlation function is a measure of the Walsh codes to reject other Walsh codes in a multi-user environment (see *Figure 3.2*). From *Figure 3.2* it is evident that the Walsh sequences have excellent periodic cross-correlation properties, meaning that two codes do not interfere with each other for all time shifts τ, since they are perfectly orthogonal, i.e. super-orhogonal in the cross-correlation function if only one sample per chip are taken. However, this result drastically deteriorates when multiple samples per chip is taken [63].

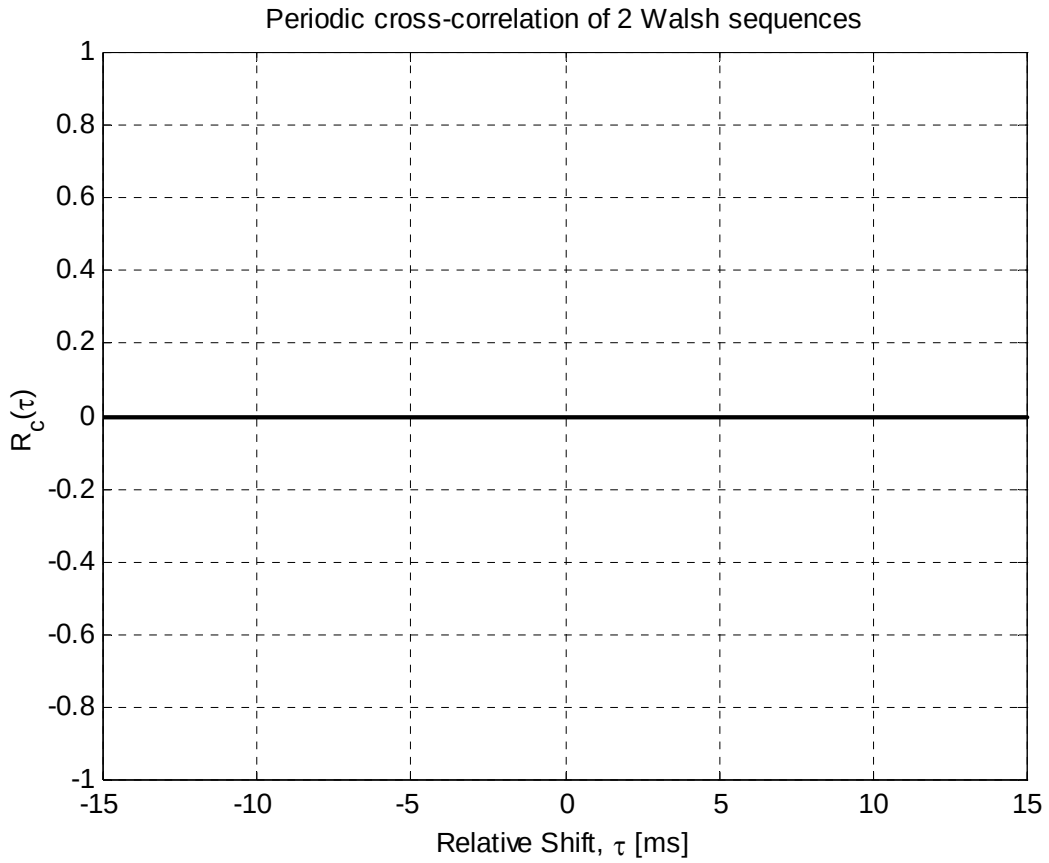

Figure 3.2 Periodic cross-correlation of two different length *N* = 16 Walsh sequences taking one sample per chip.

3.4 DIRECT SEQUENCE SPREAD SPECTRUM

A DS-SS system spreads the baseband data by directly multiplying the baseband data pulses with a pseudo-noise sequence that is produced by a pseudo-noise code generator as described in *Sections 3.1* and *3.3*. A single pulse or symbol of the spreading waveform is called a chip. The received SS signal for a single user in a DS-SS system can be represented as

$$s_{ss}(t) = \sqrt{\frac{2E_s}{T_s}}\,\mathrm{Re}\{b(t)g(t)\exp(-j2\pi f_c t + \theta)\} \qquad (3.12)$$

where E_s is the energy in the transmitted waveform, $b(t)$ is the information bit stream, $g(t)$ is the spreading sequence, f_c is the carrier frequency, and θ is the carrier phase angle at t = 0. The data waveform is a time sequence of non-overlapping rectangular pulses, each of which

has an amplitude equal to +1 or -1. Each symbol in *b(t)* represents a data symbol and has duration T_s. Each pulse in *g(t)* represents a chip, which is usually rectangular with an amplitude equal to +1 or -1, and has a duration of T_c. The transitions of the data symbols and chips occur in such a way that the ratio T_s to T_c is an integer. If B_{ss} is the bandwidth of $s_{ss}(t)$ and *BW* is the bandwidth of a conventionally modulated signal $\mathrm{Re}\{b(t)\exp(-j2\pi f_c t+\theta)\}$, the spreading due to *g(t)* results in $B_{ss} \gg BW$.

Assuming that code synchronisation has been achieved at the receiver, the received signal passes through a wideband filter and is multiplied by a local replica of the spreading sequence *g(t)*. If *g(t)* = +/- 1, then $g^2(t) = 1$, and this multiplication yields the despreaded signal $s_1(t)$ given by

$$s_1(t) = \sqrt{\frac{2E_s}{T_s}}\,\mathrm{Re}\{b(t)\exp(-j2\pi f_c t+\theta)\} \qquad (3.13)$$

at the input of the demodulator. Because $s_1(t)$ has the form of a BPSK signal, a coherent PSK demodulator can be used to extract *b(t)*. See *Figure 3.3* for a graphical representation of the waveforms and spectrums before and after spreading.

Figure 3.4 shows the received spectra of the desired SS signal and the interference at the output of the receiver wideband filter. Multiplication by the spreading waveform produces the spectra of *Figure 3.4* at the demodulator input. The signal bandwidth is reduced to *BW*, while the interference energy is spread over a RF bandwidth exceeding B_{ss}. The filtering action of the demodulator removes most of the interference spectrum that does not overlap with the signal spectrum. Thus, most of the original interference energy is eliminated by spreading and minimally affects the desired receiver signal. An approximate measure of the interference rejection capability is given by the ratio B_{ss} / *BW*, which is equal to the Processing Gain (PG) defined as

$$PG = \frac{T_s}{T_c} = \frac{R_c}{R_s} = \frac{B_{ss}}{2R_s} \qquad (3.14)$$

Thus, the greater the PG of the system, the greater will be its ability to suppress in-band interference.

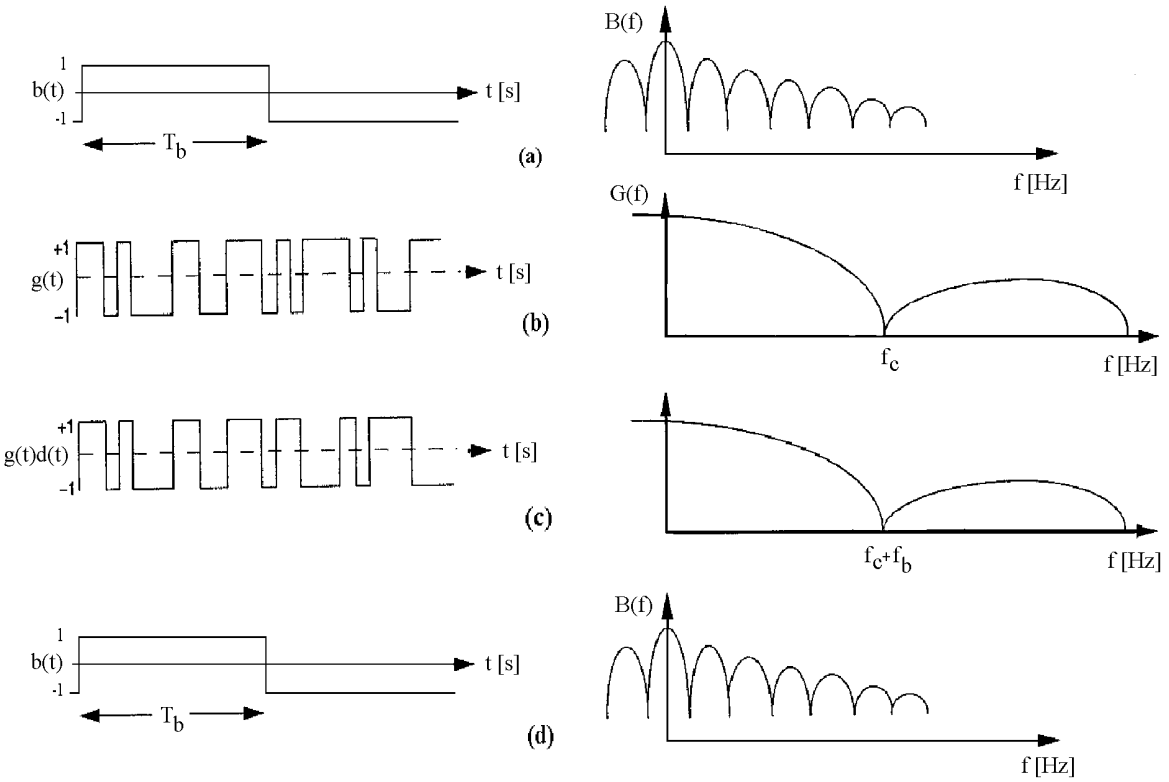

Figure 3.3. Representation of the time multiplication of a BPSK modulated signal with a spreading sequence and the resulting spectrums.

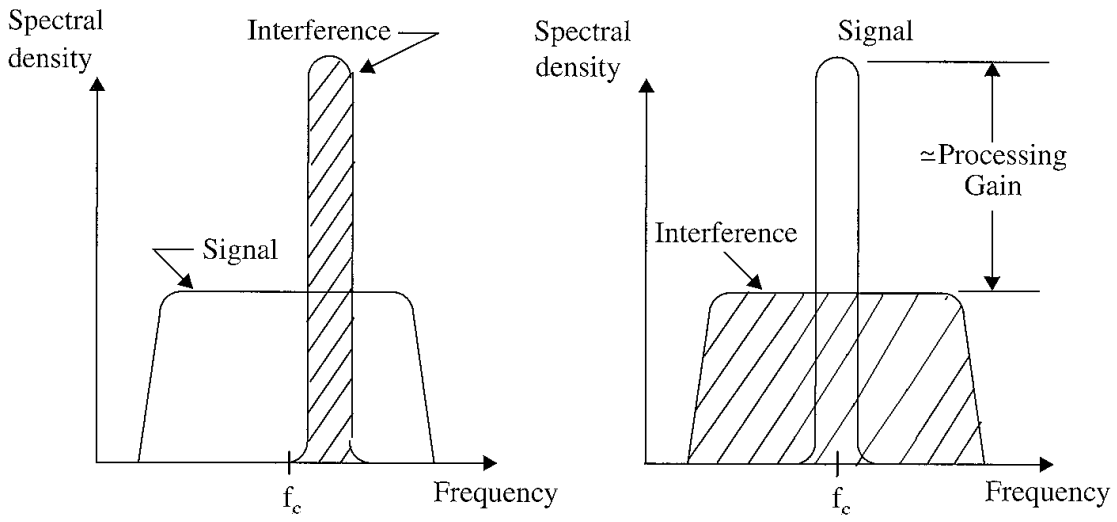

Figure 3.4. Spectra of desired received signal with interference at the wideband filter output and correlator output after despreading. Taken from [1].

3.5 PROBABILITY OF ERROR IN DS SPREAD SPECTRUM SYSTEMS

3.5.1 AWGN channel conditions

Assuming coherent demodulation in AWGN channel conditions , the probability of error for a DS-SS system employing binary PSK, is identical to the probability of error for conventional narrowband (unspreaded) binary PSK [64], that is

$$P_{e,DS-SS}^{AWGN} = Q\left(\sqrt{\frac{2E_b}{N_0}}\right) \tag{3.15}$$

where E_b denotes the energy per bit. See *Figure 3.5* for theoretical SS BER performance in AWGN channel conditions vs. flat fading channel conditions.

3.5.2 Slow Rayleigh flat fading channel conditions

Assuming coherent demodulation in slow Rayleigh flat fading channel conditions, the probability of error for a DS-SS system employing binary PSK is [17]:

$$P_{e,DS-SS}^{Rayleigh} = \frac{1}{2}\left(1-\sqrt{\frac{\frac{\bar{E}_b}{N_0}}{1+\frac{\bar{E}_b}{N_0}}}\right) \tag{3.16}$$

where $\bar{E}_b$ denotes the average energy per bit. However, this assumption is based on the fact that the fading is so slow that the Rayleigh distributed fading amplitude may be regarded as a constant over at least one symbol interval T_s. For purposes of comparison, SS's BER performance in slow Rayleigh fading channel conditions is also included in *Figure 3.5*. At this stage, the reader may wonder why DS-SS will experience flat fading? The answer lies in the fact that the DS-SS is not used for multiple users in this dissertation, but to create

orthogonality between the transmit antennas for a single user, therefore short spreading codes justifies the assumption of the signal bandwidth being smaller than the coherence bandwidth of the channel (see Appendix C, *section C.4.1*).

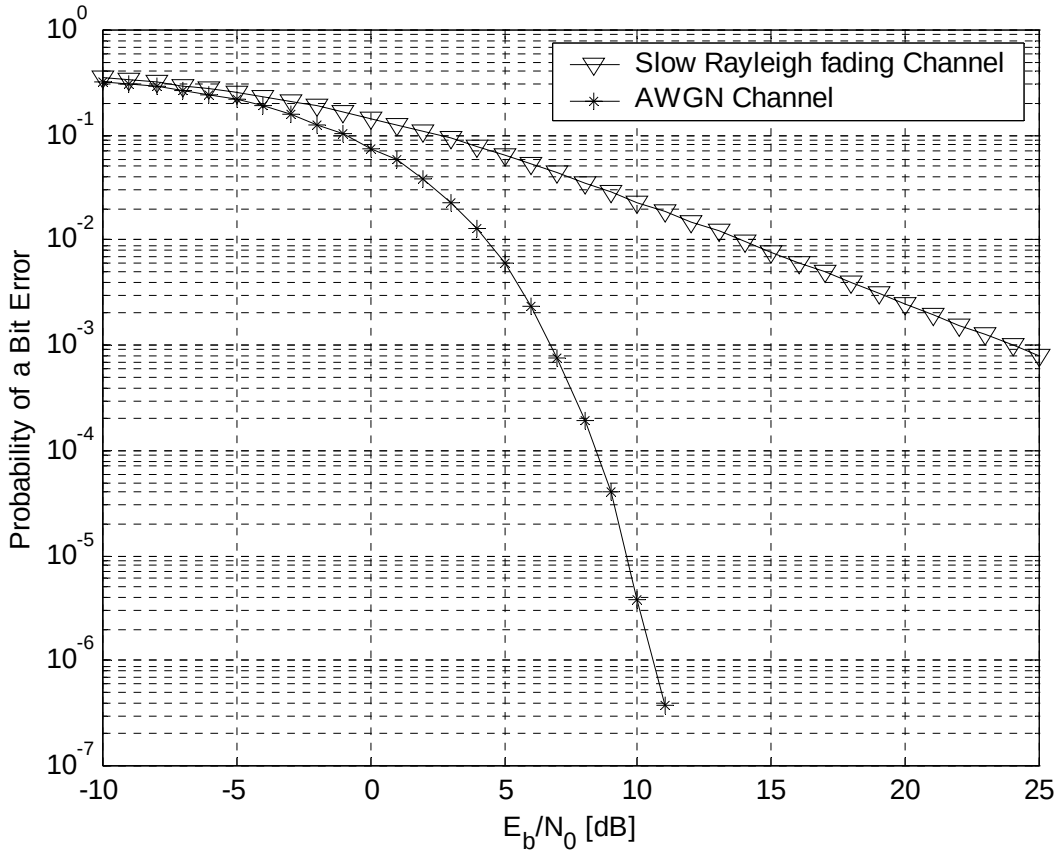

Figure 3.5. Theoretical Probability of Error vs. E_b/N_0 of a DS-SS system in flat fading channel conditions, compared to AWGN performance.

3.5.3 Multipath fading channel conditions

In [8] an approximate bit error probability is derived for RAKE receiver based DS/SSMA systems operating in a multipath environment assuming L different paths, or independent fading replicas, each having a path gain β_i. Note that the condition [4], $\sum_{i=1}^{L}(\beta_i)^2 = 1$ must be satisfied in order for the channel's output power to be equal to the input power. The probability of error is then given as

$$P_{e,DS-SS}^{multipat} = \frac{1}{2}\sum_{i=1}^{L}\left[\left(\prod_{a=1,a\neq i}^{L}\frac{\delta^i}{\delta^i-\delta^a}\right)\left(1-\sqrt{\frac{\delta^i}{1+\delta^i}}\right)\right] \tag{3.17}$$

where $\delta^i = E\left[\left(\beta_i\right)^2\right]\frac{E_b}{N_0}$.

3.6 SPACE- TIME SPREADING

STS, proposed by Hochwald *et al*. [65], is a transmit diversity technique that improves the downlink performance by using two transmit antennas at the BS and one or more antennas at the MS. However, it differs from other transmit diversity techniques in the sense that symbols are spread over multiple antennas in a way similar to ST coding. Thus, STS is a transmit diversity scheme that is based on orthogonal ST coding and combined with DS-SS. It should also be stated here that STS for the two transmit and single receive antennas was included in release A of the IS-2000 WCDMA standard.

3.6.1 General theory, real data symbols

For simplicity, assume that the normalisation factor $\sqrt{\frac{2E_s}{T_s}}$ is dropped from *Equation (3.12)* as well as the $\mathrm{Re}\{\exp(-j2\pi f_c t+\theta)\}$ term, as these two factors does not have an influence on the mathematical analysis here. *Equation (3.12)* can then be rewritten as

$$S = G \cdot B \tag{3.18}$$

where $S = s_{ss}(t)$, $G = g(t)$ and $B = b(t)$ defined in *Equation (3.19)*. Assuming n = 2, (i.e. 2 transmitter antennas are used) *Equation (3.18)* can be used in the following manner. G is a 2ς x 2 matrix consisting of two distinct spreading codes of length 2ς each. B is a 2x2 matrix consisting of the two baseband symbols to be spreaded and transmitted and S is the transmitted signals over the two transmit antennas, also represented by a 2ς x 2 matrix. Thus,

$$G = [\bar{g}_1 \quad \bar{g}_2], \qquad B = \begin{bmatrix} b_1 & b_2 \\ b_2 & -b_1 \end{bmatrix} \tag{3.19}$$

By using the channel model defined in *Chapter 2, Section 2.5, Equation (2.27)*, the received signal $\bar{r}$ at the single receive antenna is

$$\bar{r} = S\bar{h} + \bar{\eta} = GB\bar{h} + \bar{\eta} \tag{3.20}$$

where $\bar{h}$ is the complex channel conditions and $\bar{\eta}$ is the received noise. $\bar{h}$ and $\bar{\eta}$ are defined as

$$\bar{h} = \begin{bmatrix} h_1 \\ \vdots \\ h_n \end{bmatrix}, \qquad \bar{\eta} = \begin{bmatrix} \eta_1 \\ \vdots \\ \eta_n \end{bmatrix} \tag{3.21}$$

respectively. See *Chapter 4* for an in depth discussion on complex channel conditions, as well as the received noise. To recover the original transmitted signals, *Equation (3.20)* has to be despreaded by multiplying *Equation (3.20)* with G^H, which is the complex transpose of G. Note here that G^H is used in the case of a matched filter demodulator, where G^T can be used instead if detection is done by an integrate and dump demodulator. Because G^H can be used for both demodulator methods, this notation is used. Thus, multiplying *Equation (3.20)* with G^H, it can be written as

$$\begin{bmatrix} \bar{g}_1^H & \bar{g}_2^H \end{bmatrix} \bar{r} = \begin{bmatrix} \bar{g}_1^H & \bar{g}_2^H \end{bmatrix} \left(S\bar{h} + \bar{\eta} \right) = B\bar{h} + \begin{bmatrix} \bar{g}_1^H \eta_1 \\ \bar{g}_2^H \eta_2 \end{bmatrix} \tag{3.22}$$

$$= \begin{bmatrix} b_1 & b_2 \\ b_2 & -b_1 \end{bmatrix} \begin{bmatrix} h_1 \\ h_2 \end{bmatrix} + \bar{\upsilon}$$

$$\begin{bmatrix} \bar{g}_1^H & \bar{g}_2^H \end{bmatrix} \bar{r} = \begin{bmatrix} h_1 & h_2 \\ -h_2 & h_1 \end{bmatrix} \begin{bmatrix} b_1 \\ b_2 \end{bmatrix} + \bar{\upsilon}$$

$$= H\bar{b} + \bar{\upsilon} \tag{3.23}$$

where

$$H = \begin{bmatrix} h_1 & h_2 \\ -h_2 & h_1 \end{bmatrix}, \quad \bar{b} = \begin{bmatrix} b_1 \\ b_2 \end{bmatrix}, \quad \bar{\upsilon} = \begin{bmatrix} \bar{g}_1^H \eta_1 \\ \bar{g}_2^H \eta_2 \end{bmatrix} \tag{3.24}$$

Note that H can be used for the calculation of channel capacity to satisfy the condition stated in *Chapter 2, Section 2.5, Equation (2.30)*. The substreams are obtained by left-multiplying *Equation (3.23)* by H^H. In general, for n-fold diversity with n transmit antennas, the key identity that allows each user to decode each substream independently of others is

$$\mathrm{Re}\{H^H H\} = \bar{h}^H \bar{h} \cdot I \tag{3.25}$$

as described in *Section 2.3*, *Equation (2.18)*. Note that the $\mathrm{Re}\{\bullet\}$ term is included because only real data symbols are used. Thus, after multiplying *Equation (3.23)* with H^H the decoded substreams are

$$\begin{aligned} \begin{bmatrix} \bar{g}_1^H & \bar{g}_2^H \end{bmatrix} \bar{r} &= H^H H \bar{b} + H^H \bar{\upsilon} \\ &= \begin{bmatrix} |h_1|^2 + |h_2|^2 & h_1 h_2 - h_2 h_1 \\ h_2 h_1 - h_1 h_2 & |h_1|^2 + |h_2|^2 \end{bmatrix} \bar{b} + H^H \bar{\upsilon} \end{aligned} \tag{3.26}$$

Thus, taking only the real part of *Equation (3.26)*, results in

$$\begin{bmatrix} \bar{g}_1^H & \bar{g}_2^H \end{bmatrix} \bar{r} = \begin{bmatrix} |h_1|^2 + |h_2|^2 & 0 \\ 0 & |h_1|^2 + |h_2|^2 \end{bmatrix} \bar{b} + H^H \bar{\upsilon} \tag{3.27}$$

which in fact proves *Equation (3.25)*, and shows that the transmitted symbols $\bar{b} = \begin{bmatrix} b_1 \\ b_2 \end{bmatrix}$ are successfully decoded.

3.6.2 General theory, complex data symbols

By using complex data symbols at the transmitter instead of real symbols, as described above, the matrix H must obey

$$H^H H = \left(|h_1|^2 + \cdots + |h_n|^2\right) I = \bar{h}^H \bar{h} \cdot I \tag{3.28}$$

in order to decode each substream individually and provide n-fold diversity. Once again refer to *Chapter 2, Section 2.3, Equation (2.18)*. Note that *Equation (3.28)* differs from *Equation (3.25)* in the sense that the $\mathrm{Re}\{\bullet\}$ and $\mathrm{Im}\{\bullet\}$ parts are utilised. For n = 2, that can attain full diversity, the matrix H

$$H = \begin{bmatrix} h_1 & h_2 \\ -h_2^* & h_1^* \end{bmatrix} \tag{3.29}$$

which satisfies *Equation (3.28)*. By observing the product

$$\begin{aligned} H\bar{b} &= \begin{bmatrix} h_1 & h_2 \\ -h_2^* & h_1^* \end{bmatrix} \begin{bmatrix} b_1 \\ b_2 \end{bmatrix} \\ &= \begin{bmatrix} h_1 b_1 + h_2 b_2 \\ -h_2^* b_1 + h_1^* b_2 \end{bmatrix} \end{aligned} \tag{3.30}$$

it can be seen that we cannot find a B such that $H\bar{b} = B\bar{h}$, as is the case in *Equation (3.23)*, and for this reason it is unclear what we should transmit. However, if the second entry of *Equation (3.30)* is conjugated, then

$$\begin{aligned} \begin{bmatrix} h_1 b_1 + h_2 b_2 \\ -h_2^* b_1 + h_1^* b_2 \end{bmatrix} &= \begin{bmatrix} b_1 & b_2 \\ b_2^* & -b_1^* \end{bmatrix} \begin{bmatrix} h_1 \\ h_2 \end{bmatrix} \\ &= B\bar{h} \end{aligned} \tag{3.31}$$

where

$$B = \begin{bmatrix} b_1 & b_2 \\ b_2^* & -b_1^* \end{bmatrix} \tag{3.32}$$

Hence, the transmitted signal should be

$$S = G \cdot B \tag{3.33}$$

where G is defined in *Equation (3.19)* and B in *Equation (3.32)*. As in the real symbol case described in *Section 3.6.1*, the received signal $\bar{r}$ is despreaded by G^H to give

$$\begin{bmatrix} \bar{g}_1^H & \bar{g}_2^H \end{bmatrix} \bar{r} = G^H \left(S\bar{h} + \bar{\eta} \right) = B\bar{h} + \begin{bmatrix} \bar{g}_1^H \bar{\eta} \\ \bar{g}_2^H \bar{\eta} \end{bmatrix} \tag{3.34}$$

but, contrary to the real-symbol case, the second entry has to be conjugated as described by *Equation (3.31)*, to yield

$$\begin{aligned} \begin{bmatrix} \bar{g}_1^H & \bar{g}_2^H \end{bmatrix} \bar{r} &= H\bar{b} + \begin{bmatrix} \bar{g}_1^H \bar{\eta} \\ \left(\bar{g}_2^H \bar{\eta} \right)^* \end{bmatrix} \\ &= \begin{bmatrix} |h_1|^2 + |h_2|^2 & h_1^* h_2 - h_1^* h_2 \\ h_2^* h_1 - h_2^* h_1 & |h_1|^2 + |h_2|^2 \end{bmatrix} \bar{b} + H^H \bar{\upsilon} \\ &= \begin{bmatrix} |h_1|^2 + |h_2|^2 & 0 \\ 0 & |h_1|^2 + |h_2|^2 \end{bmatrix} \bar{b} + H^H \bar{\upsilon} \end{aligned} \tag{3.35}$$

where $\bar{\upsilon} = \begin{bmatrix} \bar{g}_1^H \bar{\eta} \\ \left(\bar{g}_2^H \bar{\eta} \right)^* \end{bmatrix}$. Hence, the transmitted symbols $\bar{b} = \begin{bmatrix} b_1 \\ b_2 \end{bmatrix}$ are successfully decoded.

Tarok *et al.* [13] showed that square matrices H obeying *Equation (3.28)* do not exist presently for $n > 2$, i.e. for more than 2 transmit antennas. The proposed scheme in this dissertation provides a method for obtaining full rate, full diversity for more than 2 transmit antennas.

3.7 OVERVIEW OF CURRENT ST CODING - CDMA LITERATURE

Research in the field of combining ST codes and CDMA technology have started to attract more researchers over the past few years, because of the advantages that multiple antenna systems provide in a wireless environment. Most existing transmission diversity strategies are based on Bell-Labs Layered Space-Time (BLAST) [66] or orthogonal ST block coding [65, 67]. There are three proposals in [66], i.e.

- Spreading all the symbols of one user with the same code to maximize the spectral efficiency.
- Assigning each user *n*-orthogonal spreading sequences, and then spreading each antenna's signal with its own spreading code.
- Transmitting each symbol simultaneously over *n* antennas with *n* different spreading codes, to improve the diversity gain.

For an in-depth discussion on orthogonal ST block coding [65], see *Section 3.6*.

All of the work presented in [65, 66, 67, 68, 69], apply the DS-SS technique over the codewords of conventional ST block coding, whereas CSSs are used in [70]. However, a resent publication by Doostnejad [28], proposed a two-dimensional STS code, that provides full transmit diversity and high spectral efficiency, and is based upon the principal that orthogonal user blocks are transmitted over *n* transmit antennas.

3.8 CONCLUDING REMARKS

Chapter 3 presented theoretical concepts with respect to spreading sequences. In particular, Walsh spreading sequences, known for their excellent cross-correlation properties and accordingly, the main reason for using them in this study, was discussed in detail. A brief overview of CSSs was also presented. Further, the applications of spreading sequences in DS-SS was discussed, and extended to the case where these spreading sequences are used in conjunction with ST coding techniques, generally known as STS. Lastly, recent development the research field of incorporating ST coding in CDMA platforms were discussed. Next, the mobile fading channel simulation platform is presented that was used to generate the simulation results presented in *Chapter 6*.

CHAPTER FOUR

MOBILE FADING CHANNELS

This chapter contains a concise summary of the fading channels used in the simulation platforms to generate the proposed DSSTS as well as SSTD scheme's simulation results. A typical model of a land mobile radio scenario, including Personal Communication Systems (PCS) and other digital cellular transmission links, is shown in Appendix C, *Figure C.1*. It consists of an elevated BS antenna (or multiple antennas) with a relatively short distance Line-of-Sight (LOS) propagation path, and many Non-Line-of-Sight (NLOS) reflected propagation paths towards the mobile antenna or antennas mounted on the vehicle or mobile unit. In most applications, no complete or direct LOS propagation exists between the BS antenna (also known as the access point) and the mobile antennas, because of natural and constructed obstacles (see Appendix C, *Figure C.1*). Thus, the transmitted radio waves reach the mobile unit from different directions and with different time delays, caused by the multiple paths. This scenario causes small-scale fading.

Small-scale fading, or simply fading, is used to describe the rapid fluctuations of the amplitudes, phases, or multipath delays of the radio signal over a short period of time or distance of travel. Thus, basically the time dependency of the fading is removed from the large-scale path losses in order to separate small-scale fading from large-scale fading.

Large-scale fading or path loss is the decrease in the signal's amplitude that travelled over a large distance. One popular method to calculate path losses over large distance is to use the free space propagation loss model [1].

This chapter is structured as follows: In *Section 4.1* a general overview of the Flat Fading Channel Simulator (FFCS) used in this dissertation is presented, followed by a multipath fading channel model in *Section 4.2*. Lastly, a Multipath Fading Channel Simulator (MFCS) are presented in *Sections 4.3*. Also see Appendix C and D for an in depth discussion on all multipath fading signal propagation effects.

4.1 FLAT FADING CHANNEL SIMULATOR MODEL

4.1.1 Description of the slow/fast fading channel simulator

A popular method of simulating a channel is by means of the classic *Clarke* FFCS, which is presented in Appendix D. However, the use of the Hilbert transform in a classic *Clarke* FFCS can be negated, as shown by Staphorst [17], by assuming that the signal components entering the fading channel has already been decomposed into real and imaginary baseband parts.

$$u(t) = \mathrm{Re}\{u(t)\} + j \cdot \mathrm{Im}\{u(t)\} \tag{4.1}$$

Thus, keeping the $\mathrm{Re}\{\ \}$ and $\mathrm{Im}\{\ \}$ branches apart, a complex flat fading process is given in *Equation (4.2)*:

$$h(t) = \alpha(t) \cdot \cos(\phi(t)) + j \cdot \alpha(t) \cdot \sin(\phi(t)) \tag{4.2}$$

where $\alpha(t)$ and $\phi(t)$ are the instantaneous fading amplitude and phase of the fading channel, respectively. In order to switch the channel's fading amplitude between a Rayleigh and Rician amplitude fading distributions, a constant $\sqrt{2K}$ is added to the $\mathrm{Re}\{\ \}$ branch of the fading channel simulator . Adding the $\sqrt{2K}$ component, to *Equation (4.2)* yields,

$$h(t) = \alpha(t) \cdot \cos(\phi(t)) + \sqrt{2K} + j \cdot \alpha(t) \cdot \sin(\phi(t)) \tag{4.3}$$

Defining *d(t)* as the output from the complex channel simulator, the complex input signal *u(t)* has to be multiplied by the fading channel *h(t)* in order to produce a fading output *d(t)*, thus

$$d(t) = u(t) \cdot h(t) \tag{4.4}$$

Substituting *Equations (4.1)* and *(4.3)* into *(4.4)*, results in:

$$\mathrm{Re}\{d(t)\} = \mathrm{Re}\{u(t)\} \cdot \mathrm{Re}\{h(t)\} - \mathrm{Im}\{u(t)\} \cdot \mathrm{Im}\{h(t)\} \tag{4.5}$$

and:

$$\mathrm{Im}\{d(t)\} = \mathrm{Re}\{h(t)\} \cdot \mathrm{Im}\{u(t)\} + \mathrm{Re}\{u(t)\} \cdot \mathrm{Im}\{h(t)\} \tag{4.6}$$

respectively, that represents the $\mathrm{Re}\{\bullet\}$ and $\mathrm{Im}\{\bullet\}$ outputs of the flat fading channel, operating on a complex input signal. The complex FFCS's realisation of the *Clarke*'s flat fading channel from *Equations (4.5)* and *(4.6)* are shown in *Figure 4.1*. From this figure it is clear that:

$$\mathrm{Re}\{d(t)\} = C_{SCALE}\left[\left(n_I(t) + \sqrt{2K}\right) \cdot \mathrm{Re}\{u(t)\} - n_I(t) \cdot \mathrm{Im}\{u(t)\}\right] \tag{4.7}$$

and:

$$\mathrm{Im}\{d(t)\} = C_{SCALE}\left[\left(n_I(t) + \sqrt{2K}\right) \cdot \mathrm{Im}\{u(t)\} + n_I(t) \cdot \mathrm{Re}\{u(t)\}\right] \tag{4.8}$$

where $n_I(t)$ and $n_Q(t)$ are the respective outputs of Doppler filters $DF_I(f)$ and $DF_Q(f)$ for Gaussian input signals. It is also assumed that the Gaussian input signals have zero mean and unit variance. The constant C_{SCALE} is chosen such that the channel simulator's input signal power and output signal power are equal in magnitude. It is given by the following expression:

$$C_{SCALE} = \frac{1}{\sqrt{2(1+K)}} \tag{4.9}$$

The Rician constant K defines the ratio between the *LOS* signal strength σ_{LOS}^2 and scatter signal strength σ_{NLOS}^2 (*NLOS*). Thus,

$$K = \left[\frac{\sigma_{LOS}^2}{\sigma_{NLOS}^2} \right] \tag{4.10}$$

By using *Equation (4.10)*, it can be shown that the component added to the $\mathrm{Re}\{\ \}$ branch is given by

$$CLOS = \sqrt{2K} \tag{4.11}$$

See Appendix D for the derivation of *Equations (4.9)* and *(4.11)*.

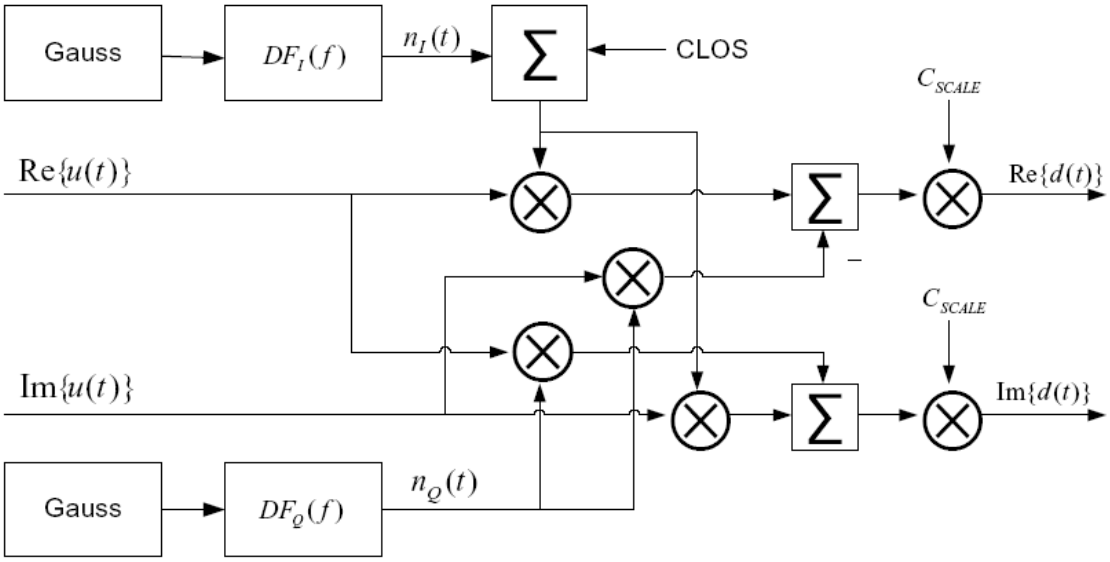

Figure 4.1. Clarke's model for a Complex FFCS employing both Rayleigh and Rice fading.

4.2 MULTIPATH FADING CHANNEL MODEL

The multipath fading phenomenon is primarily a result of the time variations in the phases of received signals at the receiver through *L*-paths. The received signal in the case of a discrete multipath channel is given by *Equation (4.12),*

$$d(t) = \sum_{i=1}^{L} \beta_i(t) \exp\left(-\, j\vartheta_i(t)\right) \qquad (4.12)$$

where $\theta_i(t) = 2\pi f_c \tau_i(t)$, $\tau_i(t)$ is the time delay associated with the *i*'th path of the multipath channel and $\beta_i(t)$ is the amplitude of the *i*'th path of the multipath channel (see Appendix D.3 for the derivation of *Equation 4.12*). Thus at time *t*, the received signal consists of the sum of a number of time-variant vectors (phasors) having amplitudes $\beta_i(t)$ and phases $\theta_i(t)$. That is, at times the randomly time-variant phases $\theta_i(t)$ associated with the vectors $\{\beta_i \exp(-j\theta_i)\}$ result in the vectors adding destructively (see Appendix C, *Figure C.2*). When this occurs, the resultant received signal $d(t)$ is very small or practically zero. At other times, the vectors $\{\beta_i \exp(-j\theta_i)\}$ add constructively, so that the received signal is large (see Appendix C, *Figure C.2*). Thus, the amplitude variations in the received signal, termed signal fading, are due to the time-variant multipath characteristics of the channel. Also note that the delays $\tau_i(t)$, associated with the different signal paths, will also change at different rates and in an unpredictable manner.

Two characteristics of a time-varying multipath channel are the introduction of delay spread, and the nature of all multipaths vary with time in accordance with the environmental changes. The time variations in the channel appear to be unpredictable to the user of the channel and for this reason, a time variant multipath channel is characterised statistically. For a more in depth discussion on the statistical analysis of a multipath fading channel, see Appendix D. A common term usually associated with multipath fading channels is the multipath power delay profile shown in *Figure 4.2.*

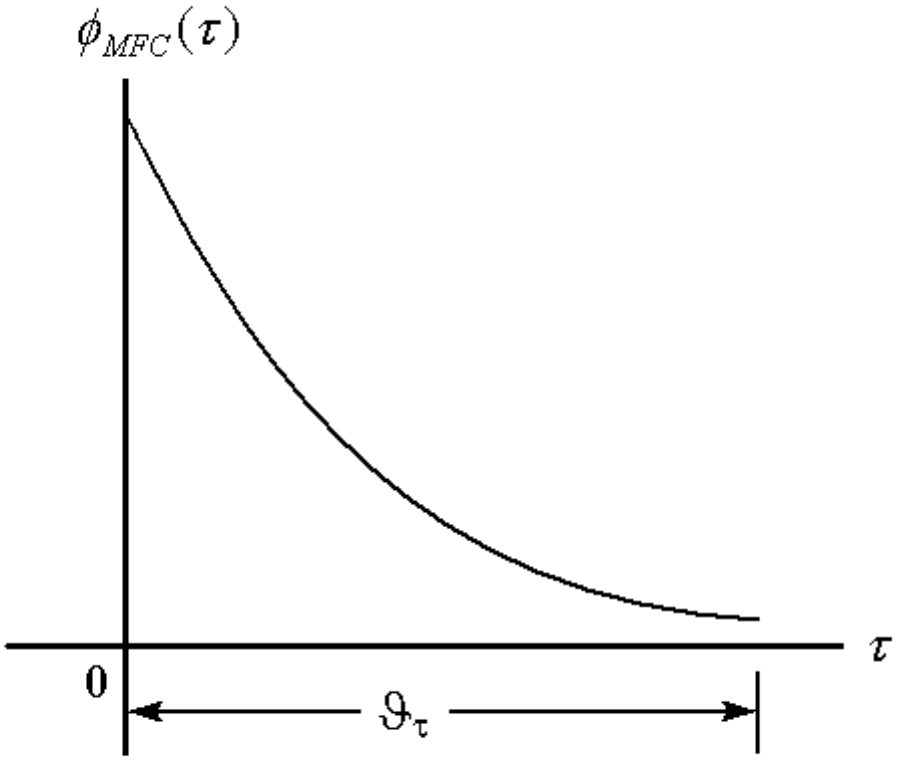

Figure 4.2 Multipath power delay profile with a delay spread of ϑ_τ.

In practice, the multipath power delay profile is measured by transmitting very narrow pulses or, equivalently, a wideband signal and cross-correlating the received signal with a delayed version of itself. The measured cross-correlation function of the multipath fading channel $\Phi_{MFC}(\tau)$ may appear as shown in *Figure 4.2* (see Appendix D). The range of values of τ over which $\Phi_{MFC}(\tau)$ is nonzero, or above a certain threshold, is called the delay spread ϑ_τ of the channel. As described in Appendix C, *Section C.4*, the delay spread ϑ_τ vs. the transmitted signal period determines whether the channel's fading is flat or frequency selective.

4.3. MULTIPATH FADING CHANNEL SIMULATOR MODEL

A flat or frequency selective fading channel, as described in *Section 4.2*, can be simulated using the general MFCS structure as shown in *Figure 4.3*. This simulator is capable of simulating a time-invariant multipath fading channel, consisting of *L* discrete and independently faded multipath components.

To simulate an appropriate power delay profile with the MFCS, *L*-paths are selected with their respective delays, denoted by τ_i. Next, each delayed version of the input signal is scaled by β_i to represent the average amplitude on the *i*'th path of the multipath channel. These delayed and scaled signals are then processed by *L*-FFCS, denoted as *FFCS 1* to *FFCS L* in *Figure 4.3*. Note that this approach allows the power delay profile to be configured such that each *i*'th path can be processed with its own unique Doppler frequency and Rician constant. The resultant outputs from the *L*-FFCS are then added to produce the output from the MFCS, denoted as *d(t)*. Recall from *Section 3.4.3*, that it is important that the condition, $\sum_{i=1}^{L}(\beta_i)^2 = 1$ must be satisfied in order for the channel's output power to be equal to the input power [4].

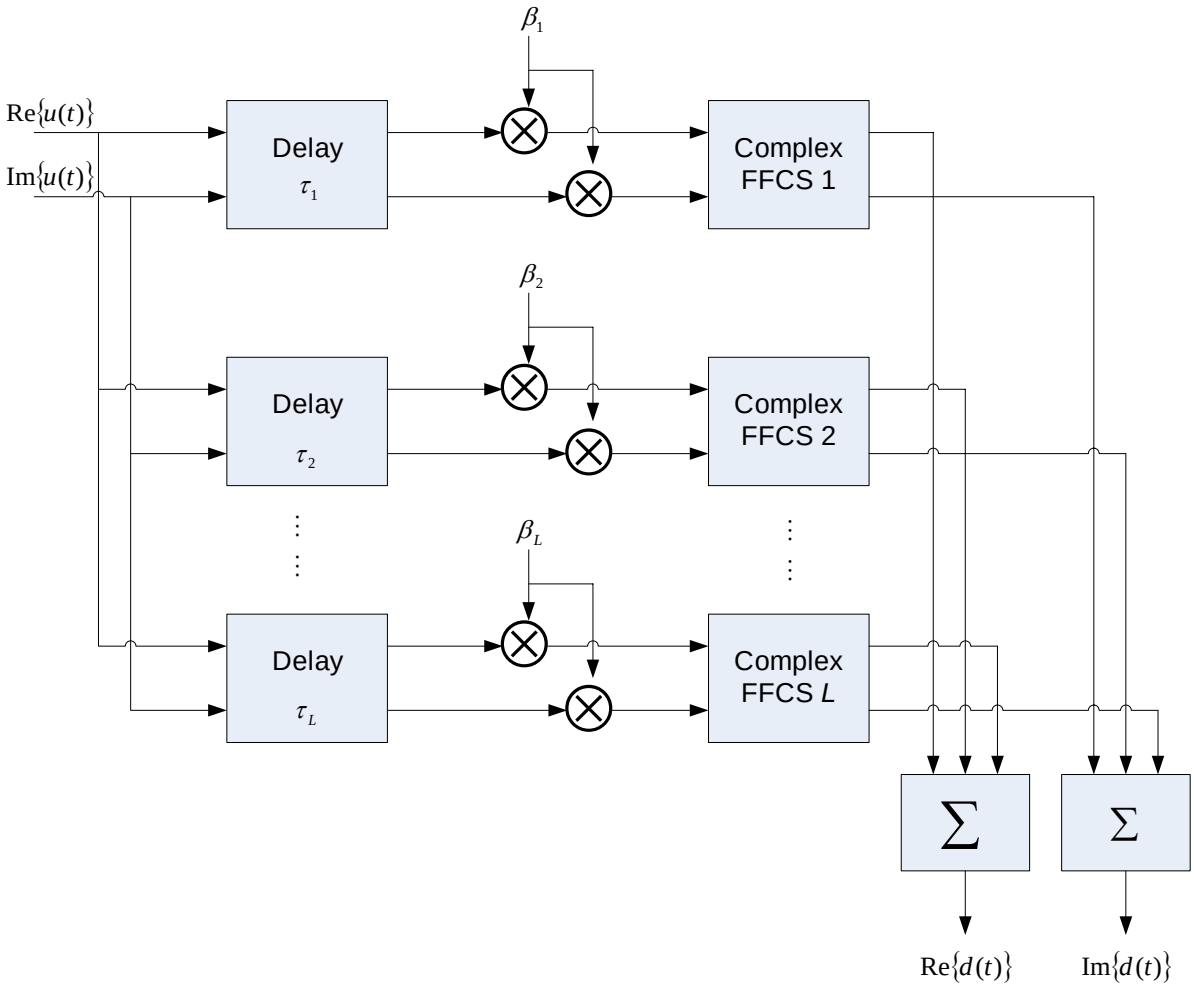

Figure 4.3 MFCS with *L* discrete and independently faded paths employing *L*-FFCS and *L*-time delays.

CHAPTER FIVE

PROPOSED SPACE-TIME SPREADING SCHEMES

In *Chapter 2* a communication system was presented that consisted of a BS with n transmit antennas (were $n = 2$) and a MS with only one receive antenna. In Chapter 5, a scheme to increase the number of transmit antennas at the BS to more than two transmit antennas is proposed. Although other schemes have been proposed that accomplished this (see *Chapters 2* and *3*), these schemes cannot achieve full rate and full diversity for more than 4 transmit antennas. As stated in the introduction, an objective of this study is to find a method of increasing the number of transmit antennas at the BS from two transmit antennas to an arbitrary number of transmit antennas that achieve both full rate and full diversity. This objective is met by the proposed scheme and referred to as DSSTS. Although only one receive antenna is assumed in this particular study, it can easily be extended to multiple receive antennas.

This chapter is structured as follows: In *Sections 5.1,* a general overview of the DSSTS scheme's transmission model, encoding and decoding algorithms are presented. Further,

the effect of non-perfect cross-correlation of spreading sequences at the receiver is analysed, the capacity for the DSSTS scheme is derived and the simulation platform used in this dissertation is presented. Lastly, the focus of *Section 5.2* is on a SSTD scheme presented in Maasdorp *et al*. [19, 20] to relieve Alamouti's ST decoding scheme from the assumption that the channel has to be quasi-static.

5.1 DIRECT SEQUENCE SPACE-TIME SPREADING SCHEME

5.1.1 DSSTS transmission model

The proposed DSSTS scheme that achieves full rate and full diversity is presented in *Figure 5.1*. It consists of the following building blocks:

- A symbol mapping function, for example QPSK, QAM etc,
- a cyclic shift register that shift symbols two symbols positions at even time periods, i.e. t = 2, 4, 6, …,
- y (2 x 2) Alamouti matrices from *Equation 5.1* and
- y orthogonal spreading codes.

Note that the number of ST block codes and spreading codes utilized in the DSSTS scheme will always be equal to $n/2$. Thus, $y = n/2$. It should also be stated here that any spreading code family could be used in the DSSTS scheme. Since perfect synchronization is assumed in this study, only the cross-correlation properties of the spreading sequences are important. Cross-correlation, as well as auto-correlation properties, were discussed in detail in *Chapter 3, Section 3.3*. As Walsh sequences have excellent periodic cross-correlation properties, it was the choice for this study. However, for real-life implementation, other spreading sequences that have excellent cross- as well as auto-correlation properties, for example CSSs, may be considered (See *Chapter 3, Section 3.2* for more information on CSSs).

For simplicity, only a QPSK symbol constellation is assumed, but any other possible symbol constellation can also be used. By using a QPSK symbol constellation, two incoming bits, b_1 and b_2 from bitstream $\bar{b}$, are mapped to a single symbol, presented as $[b_1 b_2] \rightarrow a_1$ from the

symbol constellation ν. Thus, if n transmit antennas are used, a block of $2n$ bits are mapped to n symbols, presented as a_1 to a_n. These mapped symbols, presented in matrix form as $[b_1 b_2 \quad b_3 b_4 \quad \cdots \quad b_{2n-1} b_{2n}]^T \rightarrow [a_1 \quad a_2 \quad \cdots \quad a_n]^T$, are shown in *Figure 5.1*. These n symbols are then shifted into the cyclic symbol shift register and shifted by 2 symbol positions after 2 time slots over a total of l time slots. The reason for the 2 symbol position shifts after every 2 time slots are as follows:

- Each of the y ST encoder blocks in *Figure 5.1* has an Alamouti matrix, see *Chapter 2, Section 2.2.2, Equation (2.4).* Note that $y = n/2$.
- At the first time slot t_1, the symbols in row one of *Equation (2.4)* are the output of the y'th ST-encoder.

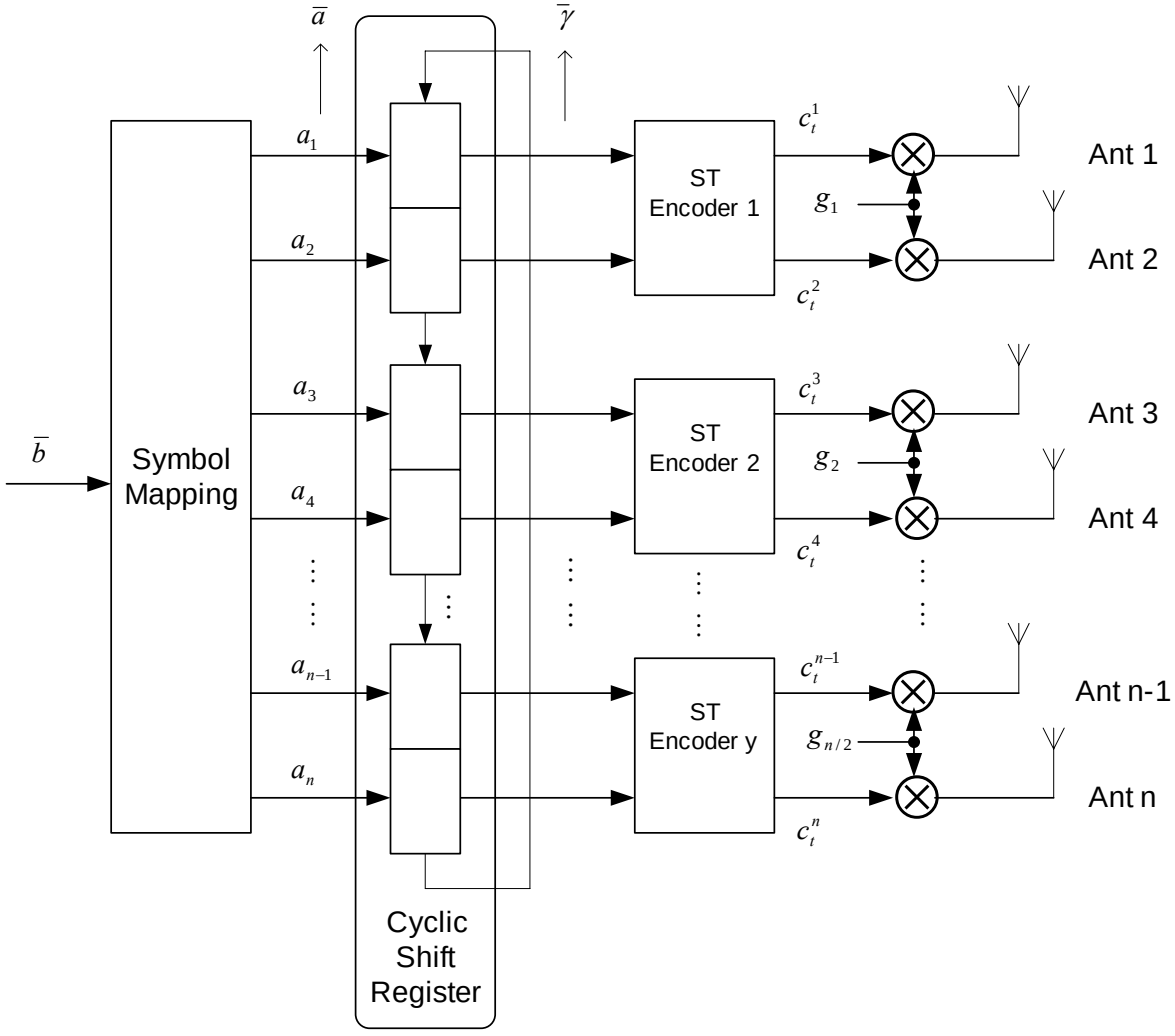

Figure 5.1. Proposed DSSTS transmitter structure, achieving full rate and full diversity.

- At the second time slot t_1+T_s, where T_S is the symbol period, the symbols in row two of *Equation (2.4)* are the output of the *y*'th ST-encoder.
- Thus, for every 2 input symbols at the *y*'th ST-encoder, 2 sets of 2 encoded symbols are present at the output after 2 time slots. For this reason the 2 input symbols at every *y*'th ST-encoder has to be shifted 2 symbols positions at every second time slot.

The output of the shift register, γ, for n symbols and $t = 1$ to l, can be shown in matrix form as:

$$\bar{\gamma} = \begin{bmatrix} \bar{\gamma}_1 & \bar{\gamma}_2 & \cdots & \bar{\gamma}_{l-1} & \bar{\gamma}_l \end{bmatrix} = \begin{bmatrix} a_1 & a_2 & \cdots & \cdots & a_{n-1} & a_n \\ a_1 & a_2 & \cdots & \cdots & a_{n-1} & a_n \\ a_{n-1} & a_n & a_1 & a_2 & \cdots & \cdots \\ a_{n-1} & a_n & a_1 & a_2 & \cdots & \cdots \\ \vdots & \vdots & \vdots & \vdots & \ddots & \vdots \\ \cdots & \cdots & a_{n-1} & a_n & a_1 & a_2 \end{bmatrix}^T \tag{5.1}$$

Note that the number of columns in *Equation (5.1)* represent the number of transmit antennas used, and that the number of rows represent the number of time periods, i.e. *l*-time slots. Also note that two consecutive time periods are the same, because the symbols are only shifted every second time slot.

For each time slot $t = 1, 2, 3, \ldots, l$, the shifted symbols $\bar{\gamma}_t$, are ST encoded (see *Section 5.2*). These ST encoded symbols c_t^i, $i = 1, 2, 3, \ldots..,n$, are then spreaded with a spreading code g_y, $y = 1, 2, 3\ldots\ldots, n/2$ and transmitted from n transmit antennas. Note that only one spreading code is used per ST block code. This is an advantage over STS schemes, presented in [27] because 50% less spreading codes are used in this scheme.

Using the same channel assumptions as in *Chapter 2*, i.e. a flat fading channel, the path gains are complex Gaussian random variables and the channel is constant over a frame length *l*, the received signal in *Figure 5.2* is

$$r_t = \sum_{i=1}^{n/2} \left(h_{2i-1}\, c_t^{2i-1} g_i + h_{2i}\, c_t^{2i} g_i \right) + \eta_t \tag{5.2}$$

where h_{2i-1} and h_{2i} are respectively defined as the path gains from transmit antennas ($2i$-1) and ($2i$) to the receive antenna and η_t is a zero mean complex Gaussian random variable. For a more detailed discussion on how h_i is defined, see *Chapter 4, Section 4.1*.

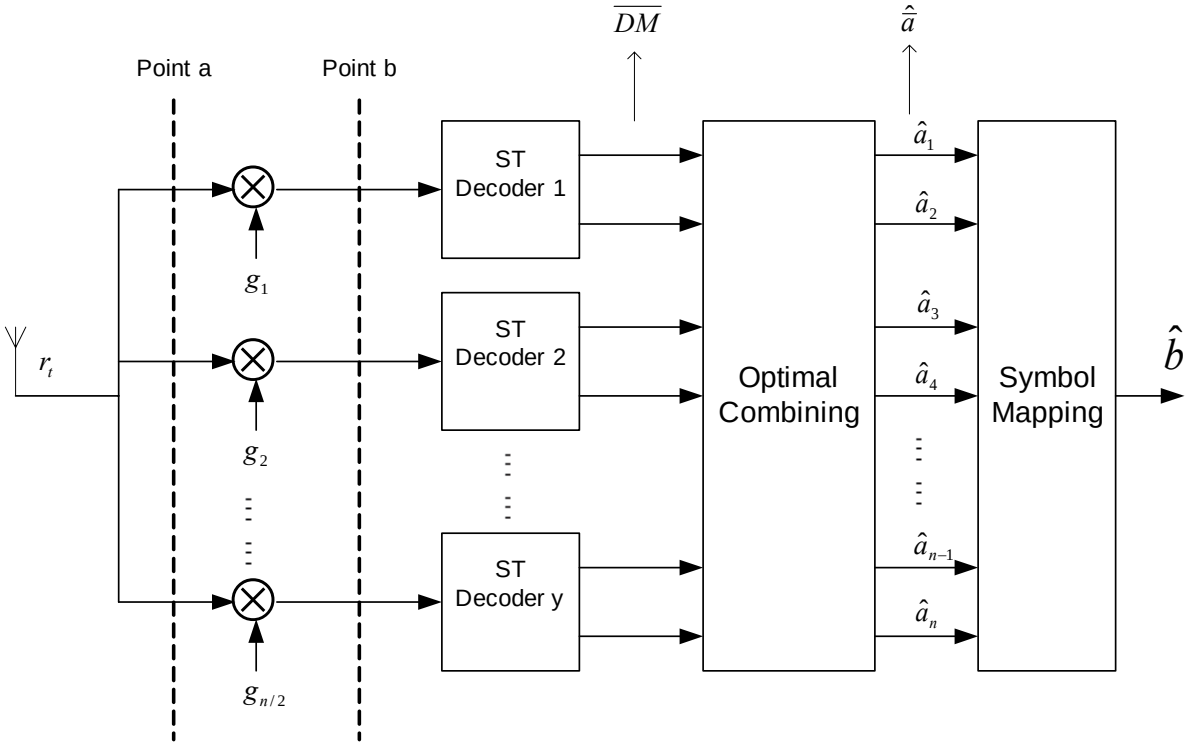

Figure 5.2. DSSTS receiver model.

Each received symbol stream r_t is despreaded with *Equation (5.3)*, i.e. point b in *Figure 5.2*.

$$\Delta_t^y = r_t g_y \qquad \text{where } y=1, 2, 3, \ldots..n/2, \quad \text{and } t = 1, 2, \ldots\ldots l \qquad (5.3)$$

Assuming perfect CSI is available after despreading, (point b in *Figure 5.2*) the receiver has to compute the decisions metrics

$$DM_j^y\Big|_{a_n} = \sum_{t=j-1}^{t+1} \left| \Delta_t^y - \sum_{i=y} \left(h_{2i-1}\, c_t^{2i-1} + h_{2i}\, c_t^{2i} \right) \right|^2 \qquad \text{for j = 2, 4, 6, ..,} l \qquad (5.4)$$

where *y* represents the ST decoder index and a_n represents one of *n* transmitted symbols. The decisions metrics are computed over all code words

$$c = \begin{bmatrix} c_1^1 & c_2^1 & \cdots & c_l^1 \\ c_1^2 & c_2^2 & \cdots & c_l^2 \\ \vdots & \vdots & \ddots & \vdots \\ c_1^n & c_2^n & \cdots & c_l^n \end{bmatrix} \tag{5.5}$$

Note that zero periodic cross-correlation between different Walsh spreading codes in *Equation (5.5)* is assumed. This topic is discussed in more detail in *Section 5.1.4* for the case when the periodic cross-correlation between different spreading sequences is not equal to zero.

The ST-decoders compute the decision metrics from *Equation (5.4)* and the output of all *y* ST decoders from *Figure 5.2* can be written in matrix form as

$$\overline{DM} = \left[DM_j^1\big|_{a_n} \quad DM_j^2\big|_{a_n} \quad \cdots \quad DM_j^{y-1}\big|_{a_n} \quad DM_j^y\big|_{a_n} \right]^T \tag{5.6}$$

for j = 2, 4, 6, ……..*l.* Note that the ST-decoders only has an output at every second time slot, because each ML detector needs two consecutive received signals in order to decouple the symbols (see *Chapter 2, Section 2.2.3*). In *Equation (5.7)*, the optimal combiner adds the decision metrics from *Equation (5.6)* to reconstruct estimates for symbols a_1 to a_n. Note that only decision metrics that are a function of the same symbol value (denoted by subscript $DM\big|_{a_i}$ in *Equation 5.7*) are added.

$$\hat{a}_i = \sum_{j=1}^{l/2} DM_{2j}^{t_{i,j}}\Big|_{a_i} \qquad \text{for } i = 1,2,3,\ldots\ldots,n \tag{5.7a}$$

$$\text{where } \iota = \begin{bmatrix} \iota_{1,1} & \iota_{1,2} & \cdots & \iota_{1,l/2} \\ \iota_{2,1} & \iota_{2,2} & \cdots & \iota_{2,l/2} \\ \iota_{3,1} & \iota_{3,2} & \cdots & \iota_{3,l/2} \\ \iota_{4,1} & \iota_{4,2} & \cdots & \iota_{4,l/2} \\ \vdots & \vdots & \ddots & \vdots \\ \iota_{n-1,1} & \cdots & \cdots & \iota_{n-1,l/2} \\ \iota_{n,1} & \cdots & \cdots & \iota_{n,l/2} \end{bmatrix} = \begin{bmatrix} 1, & 2, & \cdots & l/2 \\ 1, & 2, & \cdots & l/2 \\ l/2, & 1, & \cdots & (l-1)/2 \\ l/2, & 1, & \cdots & (l-1)/2 \\ \vdots & \vdots & \ddots & \vdots \\ 2, & \cdots & l/2, & 1 \\ 2, & \cdots & l/2, & 1 \end{bmatrix} \quad (5.7b)$$

Note the ι is a matrix with $\iota_{i,j}$ the *j*'th element in the *i*'th row. These soft symbol estimates, denoted as $\hat{a}_1$ to $\hat{a}_n$, are then mapped back to a bitstream $\hat{\hat{b}} = \left[\hat{b}_1 \hat{b}_2 \cdots \hat{b}_{2n-1} \hat{b}_{2n}\right]$ to form an estimate of the original transmitted bitstream.

5.1.2 DSSTS encoding algorithm

The new DSSTS scheme uses the Alamouti C_2 matrix, defined in *Chapter 2, Section 2.2.2, Equation (2.4)*, as building blocks. Note that henceforth in this dissertation, the Alamouti matrix will be defined as X_a. The reason for the change in notation is to show that the subscript *a* does not indicate the number of transmit antennas anymore, but is rather used as a substitution variable. In the new DSSTS scheme the Alamouti ST block codes X_a that are being spread with Walsh spreading codes g_y are used to define a l x n transmission matrix T_n,

$$T_n = \begin{bmatrix} g_1 X_1 & g_2 X_3 & \cdots & g_{n/2} X_{n-1} \\ g_1 X_{n-1} & g_2 X_1 & & \vdots \\ \vdots & & \ddots & \\ g_1 X_3 & \cdots & & g_{n/2} X_1 \end{bmatrix} \quad (5.8)$$

where each of the X_1, X_3, ... X_{n-1} Alamouti matrix's is defined as follows

$$X_a = \begin{bmatrix} x_a & x_{a+1} \\ -x_{a+1}^* & x_a^* \end{bmatrix} \quad (5.9)$$

Note that *Equation (5.9)* and *(2.4)* are exactly the same, except for the change in notation.

For example, transmission matrix T_4 in *Equation (5.8)* represents a code that utilizes four transmit antennas, as seen by the number of columns in T_4, and occurs over 4 frame lengths, i.e. $l = 4$, as seen by the number of rows in T_4. Thus, by substituting $n = 4$ into *Equation (5.8)*, *Equation (5.10)* is obtained.

$$T_4 = \begin{bmatrix} g_1 X_1 & g_2 X_3 \\ g_1 X_3 & g_2 X_1 \end{bmatrix} \tag{5.10}$$

By using *Equation (5.9)* to define X_1 and X_3 in *Equation (5.10)*, X_1 and X_3 is given by:

$$X_1 = \begin{bmatrix} x_1 & x_2 \\ -x_2^* & x_1^* \end{bmatrix} \text{ and } X_3 = \begin{bmatrix} x_3 & x_4 \\ -x_4^* & x_3^* \end{bmatrix} \tag{5.11}$$

Note that g_1X_1, g_1X_3 are transmitted from transmit antennas 1 and 2, respectively and g_2X_3, g_2X_1 are transmitted from transmit antennas 3 and 4, respectively. Orthogonality between the different Alamouti ST block codes are achieved by the spreading codes g_y,for y = 1,2,3,……n/2.

The selection of the transmitted symbols are the same as for the Alamouti ST block code presented in *Chapter 2, Section 2.2.2*. Transmission occurs in baseband and a QPSK signal constellation is employed with 2^q elements, $q = 2$. At time slot t = 1, nq bits arrive at the symbol mapping function and select signal constellation points a_1, a_2, a_3,…,a_n. The transmission matrix T_n is then formed by setting $x_i = a_i$ for i = 1, 2, 3, …,n in *Equation (5.11)* and substituting it into *Equation (5.10)*. These signal constellation points are thus spreaded with $g_{n/2}$ spreading codes and transmitted from the n transmit antennas. Since l time slots are used to transmit n symbols, the code rate can be defined as

$$R_c = n/l \tag{5.12}$$

Note that the code rate will always be equal to one, because the transmission matrix T_n is set up such that $l = n$ for all possible scenarios in the new DSSTS scheme.

An example of using six transmit antennas are given in order to explain the full rate, full diversity principle. Using the DSSTS scheme as given in *Figure 5.1* with n = 6, the transmitted symbols from the six antennas over six periods of time are given in *Figure 5.3*. The encoding procedure is as follow:

1. Symbols 1 to 6 are transformed by the Alamouti matrixes, spreaded by the Walsh codes and transmitted over two time periods.
2. Symbols 1 to 6 are then rotated over two symbol positions, such that each symbol pair is processed by a different Alamouti matrix (see *Figure 5.1*) and transmitted.
3. Step 1and 2 are repeated 3 times in the case of the six transmit antennas, so that every Alamouti matrix transforms each symbol pair.

Time	**1**	**2**	**3**	**4**	**5**	**6**
Ant1	$a_1 g_1$	$-a_2^* g_1$	$a_5 g_1$	$-a_6^* g_1$	$a_3 g_1$	$-a_4^* g_1$
Ant2	$a_2 g_1$	$a_1^* g_1$	$a_6 g_1$	$a_5^* g_1$	$a_4 g_1$	$a_3^* g_1$
Ant3	$a_3 g_2$	$-a_4^* g_2$	$a_1 g_2$	$-a_2^* g_2$	$a_5 g_2$	$-a_6^* g_2$
Ant4	$a_4 g_2$	$a_3^* g_2$	$a_2 g_2$	$a_1^* g_2$	$a_6 g_2$	$a_5^* g_2$
Ant5	$a_5 g_3$	$-a_6^* g_3$	$a_3 g_3$	$-a_4^* g_3$	$a_1 g_3$	$-a_2^* g_3$
Ant6	$a_6 g_3$	$a_5^* g_3$	$a_4 g_3$	$a_3^* g_3$	$a_2 g_3$	$a_1^* g_3$

Figure 5.3. Transmitted symbols from the six transmit antennas from figure 5.1 over six time periods.

From *Figure 5.3* it is evident that 6 symbols are transmitted from each one of the 6 transmit antennas (n = 6), hence giving the scheme full diversity. Six symbols are also transmitted over 6 time periods (l = 6), hence resulting in full rate by using *Equation (5.12)*.

5.1.3 DSSTS decoding : Disregarding spreading sequences

By using the same ML decoding scheme described in *Chapter 2, Section 2.2.3*, combined with despreading, only linear processing at the receiver is required in order to decode the received code words.

The decoding algorithm is explained by means of an example: Consider the ST block code T_4, defined in *Equation (5.10)*. Assuming that a QPSK symbol constellation with 2^q elements is used, $nq = 8$ bits from $\bar{b}$ arrive at the encoder, and select 4 complex symbols a_1, a_2, a_3 and a_4, as described in the *Section 5.2*. These four symbols are spreaded using spreading codes g_1 and g_2. The spreaded symbols, a_1g_1, a_2g_1, a_3g_2 and a_4g_2 are then transmitted simultaneously from antennas 1 to 4, respectively, as shown in the transmit matrix T_4 in *Equation (5.13)*. At the second, third and fourth time slots, the symbols form *Equation (5.13)*'s 2nd, 3rd, and 4th row are respectively transmitted.

$$T_4 = \begin{bmatrix} a_1g_1 & a_2g_1 & a_3g_2 & a_4g_2 \\ -a_2^*g_1 & a_1^*g_1 & -a_4^*g_2 & a_3^*g_2 \\ a_3g_1 & a_4g_1 & a_1g_2 & a_2g_2 \\ -a_4^*g_1 & a_3^*g_1 & -a_2^*g_2 & a_1^*g_2 \end{bmatrix} \tag{5.13}$$

The received symbol streams r_t are then despreaded by means of *Equation (5.3)* to obtain Δ_1 to Δ_4 given in *Equation (5.14)*

$$\Delta_1^1 = r_1g_1 \quad \text{and} \quad \Delta_1^2 = r_1g_2 \tag{5.14a}$$

$$\Delta_2^1 = r_2g_1 \quad \text{and} \quad \Delta_2^2 = r_2g_2 \tag{5.14b}$$

$$\Delta_3^1 = r_3g_1 \quad \text{and} \quad \Delta_3^2 = r_3g_2 \tag{5.14c}$$

$$\Delta_4^1 = r_4g_1 \quad \text{and} \quad \Delta_4^2 = r_4g_2 \tag{5.14d}$$

where r_1 to r_4 is defined in *Section 5.4*, *Equation (5.34)* to *Equation (5.37)*. After despreading, the receiver uses *Equation (5.4)* to compute the decision metrics

$$DM_2^1\Big|_{a_n} = \sum_{t=1}^{2}\left|\Delta_t^1 - \left(h_1\, c_t^1 + h_2\, c_t^2\right)\right|^2 \tag{5.15a}$$

$$DM_2^2\Big|_{a_n} = \sum_{t=1}^{2}\left|\Delta_t^1 - \left(h_3\, c_t^3 + h_4\, c_t^4\right)\right|^2 \tag{5.15b}$$

$$DM_4^1\Big|_{a_n} = \sum_{t=3}^{4}\left|\Delta_t^1 - \left(h_1\, c_t^1 + h_2\, c_t^2\right)\right|^2 \tag{5.15c}$$

$$DM_4^2\Big|_{a_n} = \sum_{t=3}^{4}\left|\Delta_t^1 - \left(h_3\, c_t^3 + h_4\, c_t^4\right)\right|^2 \tag{5.15d}$$

over all possible codewords c_t^i. Expanding *Equation (5.15)* the following is obtained:

$$DM_2^1\Big|_{a_n} = \left|\Delta_1^1 - h_1c_1^1 - h_2c_1^2\right|^2 + \left|\Delta_2^1 - h_1c_2^1 - h_2c_2^2\right|^2 \tag{5.16a}$$

$$DM_2^2\Big|_{a_n} = \left|\Delta_1^2 - h_3c_1^3 - h_4c_1^4\right|^2 + \left|\Delta_2^2 - h_3c_2^3 - h_4c_2^4\right|^2 \tag{5.16b}$$

$$DM_4^1\Big|_{a_n} = \left|\Delta_3^1 - h_1c_3^1 - h_2c_3^2\right|^2 + \left|\Delta_4^1 - h_1c_4^1 - h_2c_4^2\right|^2 \tag{5.16c}$$

$$DM_4^2\Big|_{a_n} = \left|\Delta_3^1 - h_3c_3^3 - h_4c_3^4\right|^2 + \left|\Delta_4^1 - h_3c_4^3 - h_4c_4^4\right|^2 \tag{5.16d}$$

By using *Equation (5.13)* to see which codeword c_t^i was transmitted (note that *t* represents the row entry and *i* the column entry of *Equation (5.13)*), *Equation (5.16)*, can be rewritten as

$$DM_2^1\Big|_{a_1,a_2} = \left|\Delta_1^1 - h_1a_1 - h_2a_2\right|^2 + \left|\Delta_2^1 + h_1a_2^* - h_2a_1^*\right|^2 \tag{5.17}$$

$$DM_2^2\Big|_{a_3,a_4} = \left|\Delta_1^2 - h_3a_3 - h_4a_4\right|^2 + \left|\Delta_2^2 + h_3a_4^* - h_4a_3^*\right|^2 \tag{5.18}$$

$$DM_4^1\Big|_{a_3,a_4} = \left|\Delta_3^1 - h_1a_3 - h_2a_4\right|^2 + \left|\Delta_4^1 + h_1a_3^* - h_2a_4^*\right|^2 \tag{5.19}$$

$$DM_4^2\Big|_{a_1,a_2} = \left|\Delta_4^1 - h_3a_1 - h_4a_2\right|^2 + \left|\Delta_4^2 + h_3a_2^* - h_4a_1^*\right|^2 \tag{5.20}$$

By noting that $\overline{DM}$ is of the same form as *Equation (2.10)* in *Chapter 2*, the decoupling method described in *Chapter 2, Section 2.2.3*, can be used to decouple *Equations (5.17)* to *(5.20)* into two parts. For example, $DM_2^1\big|_{a_1,a_2}$

$$DM_2^1\big|_{a_1} = \left| \left[\left(\Delta_1^1 h_1^* + (\Delta_2^1)^* h_2\right)\right] - a_1 \right|^2 + \left(-1 + \sum_{i=1}^{2} |h_i|^2\right)|a_1|^2 \tag{5.21}$$

which is only a function of a_1, and

$$DM_2^1\big|_{a_2} = \left| \left[\left(\Delta_1^1 h_2^* - (\Delta_2^1)^* h_1\right)\right] - a_2 \right|^2 + \left(-1 + \sum_{i=1}^{2} |h_i|^2\right)|a_2|^2 \tag{5.22}$$

which is only a function of a_2. For $DM_2^2\big|_{a_3,a_4}$

$$DM_2^2\big|_{a_3} = \left| \left[\left(\Delta_1^2 h_3^* + (\Delta_1^2)^* h_4\right)\right] - a_3 \right|^2 + \left(-1 + \sum_{i=3}^{4} |h_i|^2\right)|a_3|^2 \tag{5.23}$$

which is only a function of a_3, and

$$DM_2^2\big|_{a_4} = \left| \left[\left(\Delta_1^2 h_4^* - (\Delta_1^2)^* h_3\right)\right] - a_4 \right|^2 + \left(-1 + \sum_{i=3}^{4} |h_i|^2\right)|a_4|^2 \tag{5.24}$$

which is only a function of a_4. For $DM_4^1\big|_{a_3,a_4}$

$$DM_4^1\big|_{a_3} = \left| \left[\left(\Delta_3^1 h_1^* + (\Delta_4^1)^* h_2\right)\right] - a_3 \right|^2 + \left(-1 + \sum_{i=1}^{2} |h_i|^2\right)|a_3|^2 \tag{5.25}$$

which is only a function of a_3, and

$$DM_4^1\Big|_{a_4} = \Big| \left[\left(\Delta_3^1 h_2^* - (\Delta_4^1)^* h_1\right)\right] - a_4\Big|^2 + \left(-1 + \sum_{i=1}^{2} |h_i|^2\right)|a_4|^2 \tag{5.26}$$

which is only a function of a_4. For $DM_4^2\Big|_{a_1,a_2}$

$$DM_4^2\Big|_{a_1} = \Big| \left[\left(\Delta_3^2 h_3^* + (\Delta_4^2)^* h_4\right)\right] - a_1\Big|^2 + \left(-1 + \sum_{i=3}^{4} |h_i|^2\right)|a_1|^2 \tag{5.27}$$

which is only a function of a_1, and

$$DM_4^2\Big|_{a_2} = \Big| \left[\left(\Delta_3^2 h_4^* - (\Delta_4^2)^* h_3\right)\right] - a_2\Big|^2 + \left(-1 + \sum_{i=3}^{4} |h_i|^2\right)|a_2|^2 \tag{5.28}$$

which is only a function of a_2.

By using *Equation (5.7)*, i.e. the optimal combiner in *Figure 5.2*, the receiver combines the decision metrics by adding the soft estimates of similar symbol values. Thus, for symbol a_1 to a_4, *Equation (5.7a)* can be written as

$$\hat{a}_1 = \sum_{j=1}^{2} DM_{2j}^{t_{1,j}}\Big|_{a_1} \tag{5.29}$$

that combines the soft estimate outputs from the decision metrics of *Equations (5.21)* and *(5.27)*

$$\hat{a}_2 = \sum_{j=1}^{2} DM_{2j}^{t_{2,j}}\Big|_{a_2} \tag{5.30}$$

similarly, the soft estimate outputs from the decision metrics of *Equations (5.22)* and *(5.28)* are combined to yield:

$$\hat{a}_3 = \sum_{j=1}^{2} DM_{2j}^{t_{3,j}}\Big|_{a_3} \tag{5.31}$$

The soft estimate outputs from the decision metrics of *Equations (5.23)* and *(5.25)* are combined to form:

$$\hat{a}_4 = \sum_{j=1}^{2} DM_{2j}^{\iota_{4,j}}\Big|_{a_4} \tag{5.32}$$

Lastly, the soft estimate outputs from the decision metrics of *Equations (5.24)* and *(5.26)*, are combined, where *Equation (5.7b)* can be written as:

$$\iota = \begin{bmatrix} \iota_{1,1} & \iota_{1,2} \\ \iota_{2,1} & \iota_{2,2} \\ \iota_{3,1} & \iota_{3,2} \\ \iota_{4,1} & \iota_{4,2} \end{bmatrix} = \begin{bmatrix} 1, & 2 \\ 1, & 2 \\ 2, & 1 \\ 2, & 1 \end{bmatrix} \tag{5.33}$$

Using $\hat{a}_1\ \hat{a}_2\ \hat{a}_3\ \hat{a}_4$, the symbols are mapped back to the original bitstream $\hat{\hat{b}} = \left[\hat{b}_1\hat{b}_2\cdots\hat{b}_7\hat{b}_8\right]$.

5.1.4 DSSTS decoding : Taking spreading sequences into account

As discussed in *Sections 5.1.1* and *5.1.3*, it was assumed that the spreading codes at the receiver has zero cross-correlation after despreading each stream with its corresponding spreading sequence. However, this will not always be the case with the DSSTS, since no phase corrections are done before despreading. Therefore it is necessary to look into the case when the cross-correlation between different spreading codes are non-zero, to establish what effect it will have on the performance of the DSSTS scheme. This section can be best described by means of an example. Assume the same scenario described in *Section 5.1.3*, where a 4 transmit antenna DSSTS scheme is used. Thus, the transmission matrix is given by *Equation (5.13)*.

By using the T_4 transmission matrix from *Equation (5.13)*, the received signals at the receiver are given by *Equation (5.2)* in *Section 5.1.1*, i.e. point a in *Figure 5.2*. By expanding *Equation (5.2)* and substituting the correct code word into c_t^i, the following is obtained: For t = 1,

$$r_1 = a_1 g_1 h_1 + a_2 g_1 h_2 + a_3 g_2 h_3 + a_4 g_2 h_4 + \eta_1 \quad (5.34)$$

where $a_1 = c_1^1;\ a_2 = c_1^2;\ a_3 = c_1^3$ and $a_4 = c_1^4$.

For t = 2,

$$r_2 = -a_2^* g_1 h_1 + a_1^* g_1 h_2 - a_4^* g_2 h_3 + a_3^* g_2 h_4 + \eta_2 \quad (5.35)$$

where $-a_2^* = c_2^1;\ a_1^* = c_2^2;\ -a_4^* = c_2^3$ and $a_3^* = c_2^4$

For t = 3,

$$r_3 = a_3 g_1 h_1 + a_4 g_1 h_2 + a_1 g_2 h_3 + a_2 g_2 h_4 + \eta_3 \quad (5.36)$$

where $a_3 = c_3^1;\ a_4 = c_3^2;\ a_1 = c_3^3$ and $a_2 = c_3^4$

For t = 4,

$$r_4 = -a_4^* g_1 h_1 + a_3^* g_1 h_2 - a_1^* g_2 h_3 + a_2^* g_2 h_4 + \eta_4 \quad (5.37)$$

where $-a_4^* = c_4^1;\ a_3^* = c_4^2;\ -a_1^* = c_4^3$ and $a_2^* = c_4^4$

By using *Equation (5.3)*, the received symbol streams are then depreaded by multiplying each respective stream with its corresponding spreading sequence, i.e. at point b in *Figure 5.2*. Note that *Equation (5.14)* will be examined in detail in order to show the effect of perfect and non-perfect cross correlation.

Thus, by using r_1 to r_4 from *Equations (5.34)* to *(5.37)*, the despreaded streams are,

$$\Delta_1^1 = a_1 (g_1)^2 h_1 + a_2 (g_1)^2 h_2 + a_3 g_1 g_2 h_3 + a_4 g_1 g_2 h_4 + g_1 \eta_1 \quad (5.38a)$$

$$\Delta_2^1 = -a_2^* (g_1)^2 h_1 + a_1^* (g_1)^2 h_2 - a_4^* g_1 g_2 h_3 + a_3^* g_1 g_2 h_4 + g_1 \eta_2 \quad (5.38b)$$

$$\Delta_3^2 = a_3 g_1 g_2 h_1 + a_4 g_1 g_2 h_2 + a_1 (g_2)^2 h_3 + a_2 (g_2)^2 h_4 + g_2 \eta_3 \quad (5.38c)$$

$$\Delta_4^2 = -a_4^* g_1 g_2 h_1 + a_3^* g_1 g_2 h_2 - a_2^* (g_2)^2 h_3 + a_1^* (g_2)^2 h_4 + g_2 \eta_4 \quad (5.38d)$$

$$\Delta_1^2 = a_1 g_1 g_2 h_1 + a_2 g_1 g_2 h_2 + a_3 (g_2)^2 h_3 + a_4 (g_2)^2 h_4 + g_2 \eta_1 \quad (5.38e)$$

$$\Delta_2^2 = -a_2^* g_1 g_2 h_1 + a_1^* g_1 g_2 h_2 - a_4^* (g_2)^2 h_3 + a_3^* (g_2)^2 h_4 + g_2 \eta_2 \quad (5.38f)$$

$$\Delta_3^1 = a_3 (g_1)^2 h_1 + a_4 (g_1)^2 h_2 + a_1 g_1 g_2 h_3 + a_2 g_1 g_2 h_4 + g_1 \eta_3 \quad (5.38g)$$

$$\Delta_4^1 = -b_4^* (g_1)^2 h_1 + b_3^* (g_1)^2 h_2 - b_2^* g_1 g_2 h_3 + b_1^* g_1 g_2 h_4 + g_1 \eta_4 \quad (5.38h)$$

Perfect cross correlation

In the case of perfect cross correlation $g_1 g_2 = 0$ and $(g_1)^2 = 1$, $(g_2)^2 = 1$. Thus, *Equation (5.38)* reduces to *Equation (5.39)*

$$\Delta_1^1 = a_1 h_1 + a_2 h_2 + g_1 \eta_1 \quad (5.39a)$$

$$\Delta_2^1 = -a_2^* h_1 + a_1^* h_2 + g_1 \eta_2 \quad (5.39b)$$

$$\Delta_3^2 = a_1 h_3 + a_2 h_4 + g_2 \eta_3 \quad (5.39c)$$

$$\Delta_4^2 = -a_2^* h_3 + a_1^* h_4 + g_2 \eta_4 \quad (5.39d)$$

$$\Delta_1^2 = a_3 h_3 + a_4 h_4 + g_2 \eta_1 \quad (5.39e)$$

$$\Delta_2^2 = -a_4^* h_3 + a_3^* h_4 + g_2 \eta_2 \quad (5.39f)$$

$$\Delta_3^1 = a_3 h_1 + a_4 h_2 + g_1 \eta_3 \quad (5.39g)$$

$$\Delta_4^1 = -a_4^* h_1 + a_3^* h_2 + g_1 \eta_4 \quad (5.39h)$$

As described in *Section 5.1.3,* the ML detector attempts to minimise the decision metrics given in *Equation (5.15)*. However, these metrics can be written into a form that consist of single symbols, as given in *Equations (5.21)* to *(5.28)*. By noting that the second term in *Equations (5.21)* to *(5.28)* only consists of constants, the actual performance of the detection is based on the first term, i.e. minimizing the metric. Thus, only the first term will be taken into account from here on in this particular analysis. Substituting *Equation (5.39a)* into *Equation (5.21)*, the following is obtained

$$\Delta_1^1 h_1^* + (\Delta_2^1)^* h_2$$

$$
\begin{aligned}
&= (a_1 h_1 + a_2 h_2 + g_1 \eta_1) h_1^* + \left(-a_2 h_1^* + a_1 h_2^* + g_1^* \eta_2^*\right) h_2 \\
&= a_1 |h_1|^2 + a_2 h_1^* h_2 + g_1 \eta_1 h_1^* - a_2 h_1^* h_2 + a_1 |h_2|^2 + g_1^* \eta_2^* h_2 \\
&= a_1 |h_1|^2 + a_1 |h_2|^2 + a_2 h_1^* h_2 - a_2 h_1^* h_2 + g_1 \eta_1 h_1^* + g_1^* \eta_2^* h_2 \\
&= \underbrace{\left(|h_1|^2 + |h_2|^2\right) a_1}_{S} + \underbrace{g_1 \eta_1 h_1^* + g_1^* \eta_2^* h_2}_{N} \qquad (5.40)
\end{aligned}
$$

where S denotes the signal part and N the noise part. Substituting *Equation (5.39b)* into *Equation (5.22)* the following is obtained

$$
\begin{aligned}
&\Delta_1^1 h_2^* - (\Delta_2^1)^* h_1 \\
&= (a_1 h_1 + a_2 h_2 + g_1 \eta_1) h_2^* - \left(-a_2 h_1^* + a_1 h_2^* + g_1^* \eta_2^*\right) h_1 \\
&= a_1 h_1 h_2^* + a_2 |h_2|^2 + g_1 \eta_1 h_2^* + a_2 |h_1|^2 - a_1 h_1 h_2^* - g_1^* \eta_2^* h_1 \\
&= a_2 |h_1|^2 + a_2 |h_2|^2 + a_1 h_1 h_2^* - a_1 h_1 h_2^* + g_1 \eta_1 h_2^* - g_1^* \eta_2^* h_1 \\
&= \underbrace{\left(|h_1|^2 + |h_2|^2\right) a_2}_{S} + \underbrace{g_1 \eta_1 h_2^* - g_1^* \eta_2^* h_1}_{N} \qquad (5.41)
\end{aligned}
$$

By using the same method in obtaining *Equations (5.40)* and *(5.41)*, *Equations (5.39c)* to *(5.39h)* are substituted into *Equations (5.23)* to *(5.28)*, respectively, to yield:

$$
\Delta_1^2 h_3^* + (\Delta_2^2)^* h_4 = \underbrace{\left(|h_3|^2 + |h_4|^2\right) a_3}_{S} + \underbrace{g_2 \eta_3 h_3^* + g_2^* \eta_4^* h_4}_{N} \qquad (5.42)
$$

and

$$
\Delta_1^2 h_4^* - (\Delta_2^2)^* h_3 = \underbrace{\left(|h_3|^2 + |h_4|^2\right) a_4}_{S} + \underbrace{g_2 \eta_3 h_4^* - g_2^* \eta_4^* h_3}_{N} \qquad (5.43)
$$

is obtained by substituting *Equations (5.39e)* and *(5.39f)* into *Equations (5.23)* and *(5.24)*. Also note that *Equations (5.40)* to *(5.43)* are symbols detected over $t = 1$ and $t = 2$.

At t = 3 and t = 4, *Equations (5.44)* and *(5.45)* are obtained by substituting *Equation (5.39g)* and *(5.39h)* into *Equation (5.25)* and *(5.26)*.

$$\Delta_3^1 h_1^* + (\Delta_4^1)^* h_2 = \underbrace{\left(|h_1|^2 + |h_2|^2\right)a_3}_{S} + \underbrace{g_1\eta_3 h_1^* + g_1^*\eta_4^* h_2}_{N} \tag{5.44}$$

$$\Delta_3^1 h_2^* - (\Delta_4^1)^* h_1 = \underbrace{\left(|h_1|^2 + |h_2|^2\right)a_4}_{S} + \underbrace{g_1\eta_3 h_2^* - g_1^*\eta_4^* h_1}_{N} \tag{5.45}$$

and *Equations (5.46)* and *(5.47)* are obtained by substituting *Equations (5.39e)* and *(5.39f)* into *Equations (5.27)* and *(5.28)*

$$\Delta_3^2 h_3^* + (\Delta_4^2)^* h_4 = \underbrace{\left(|h_3|^2 + |h_4|^2\right)a_1}_{S} + \underbrace{g_2\eta_1 h_3^* + g_2^*\eta_2^* h_4}_{N} \tag{5.46}$$

$$\Delta_3^2 h_4^* - (\Delta_4^2)^* h_3 = \underbrace{\left(|h_3|^2 + |h_4|^2\right)a_2}_{S} + \underbrace{g_2\eta_1 h_4^* - g_2^*\eta_2^* h_3}_{N} \tag{5.47}$$

Using *Equation (5.7)* all of the equations of similar symbols are added, i.e. *Equations (5.40)* and *(5.46)* for symbol a_1, *Equations (5.41)* and *(5.47)* for symbol a_2, *Equations (5.42)* and *(5.44)* for symbol a_3, and *Equations (5.43)* and *(5.45)* for symbol a_4.

$$\hat{a}_1 = \underbrace{\left(|h_1|^2 + |h_2|^2 + |h_3|^2 + |h_4|^2\right)a_1}_{S} + \underbrace{g_1\eta_1 h_1^* + g_1^*\eta_2^* h_2 + g_2\eta_1 h_3^* + g_2^*\eta_2^* h_4}_{N} \tag{5.48}$$

$$\hat{a}_2 = \underbrace{\left(|h_1|^2 + |h_2|^2 + |h_3|^2 + |h_4|^2\right)a_2}_{S} + \underbrace{g_1\eta_1 h_2^* - g_1^*\eta_2^* h_1 + g_2\eta_1 h_4^* - g_2^*\eta_2^* h_3}_{N} \tag{5.49}$$

$$\hat{a}_3 = \underbrace{\left(|h_1|^2 + |h_2|^2 + |h_3|^2 + |h_4|^2\right)a_3}_{S} + \underbrace{g_2\eta_3 h_3^* + g_2^*\eta_4^* h_4 + g_1\eta_3 h_1^* + g_1^*\eta_4^* h_2}_{N} \tag{5.50}$$

$$\hat{a}_4 = \underbrace{\left(|h_1|^2 + |h_2|^2 + |h_3|^2 + |h_4|^2\right)a_4}_{S} + \underbrace{g_2\eta_3 h_4^* - g_2^*\eta_4^* h_3 + g_1\eta_3 h_2^* - g_1^*\eta_4^* h_1}_{N} \qquad (5.51)$$

Note that full diversity is obtained as described in *Chapter 3, Section 3.6*. Also note that full rate is obtained since 4 symbols are decoded over 4 time periods.

Non-Perfect cross correlation

In the case of non-perfect cross correlation $g_1 g_2 \neq 0$ and $(g_1)^2 = 1$, $(g_2)^2 = 1$. Thus, *Equations (5.38)* cannot be reduced, and are substituted directly into *Equation (5.21)* to *(5.28)*. Thus, following the same reasoning as the section on perfect correlation, *Equation (5.38a)* is substituted into *Equation (5.21)*,

$$\Delta_1^1 h_1^* + (\Delta_2^1)^* h_2$$

$$= \left(a_1(g_1)^2 h_1 + a_2(g_1)^2 h_2 + a_3 g_1 g_2 h_3 + a_4 g_1 g_2 h_4 + g_1\eta_1\right)h_1^* +$$
$$\left(-a_2^*(g_1)^2 h_1 + a_1^*(g_1)^2 h_2 - a_4^* g_1 g_2 h_3 + a_3^* g_1 g_2 h_4 + g_1\eta_2\right)^* h_2$$

$$= \left(a_1|h_1|^2 + a_2 h_1^* h_2 + a_3(g_1 g_2)h_1^* h_3 + a_4(g_1 g_2)h_1^* h_4 + g_1\eta_1 h_1^*\right) +$$

$$\left(-a_2 h_1^* h_2 + a_1|h_2|^2 - a_4(g_1 g_2)^* h_2 h_3^* + a_3(g_1 g_2)^* h_2 h_4^* + g_1^*\eta_2^* h_2\right)$$

$$= \left(a_1|h_1|^2 + a_1|h_2|^2 + a_3(g_1 g_2)h_1^* h_3 + a_3(g_1 g_2)^* h_2 h_4^* + g_1\eta_1 h_1^*\right) +$$
$$\left(a_4(g_1 g_2)h_1^* h_4 - a_4(g_1 g_2)^* h_2 h_3^* + g_1^*\eta_2^* h_2\right)$$

$$= \underbrace{\left(|h_1|^2 + |h_2|^2\right)a_1}_{S} + \underbrace{a_3(g_1 g_2)h_1^* h_3 + a_3(g_1 g_2)^* h_2 h_4^* + g_1\eta_1 h_1^* +}_{N_1}$$
$$\underbrace{\left(a_4(g_1 g_2)h_1^* h_4 - a_4(g_1 g_2)^* h_2 h_3^* + g_1^*\eta_2^* h_2\right)}_{N_2} \qquad (5.52)$$

where S once again denotes the signal part, and N_1 and N_2 the first and second noise parts respectively. Substituting *Equation (5.38b)* into *Equation (5.22)* the following is obtained

$$\Delta_1^1 h_2^* - (\Delta_2^1)^* h_1$$

$$= \left(a_1 (g_1)^2 h_1 + a_2 (g_1)^2 h_2 + a_3 g_1 g_2 h_3 + a_4 g_1 g_2 h_4 + g_1 \eta_1\right) h_2^* -$$
$$\left(-a_2^* (g_1)^2 h_1 + a_1^* (g_1)^2 h_2 - a_4^* g_1 g_2 h_3 + a_3^* g_1 g_2 h_4 + g_1 \eta_2\right)^* h_1$$

$$= \left(a_1 h_1 h_2^* + a_2 |h_2|^2 + a_3 (g_1 g_2) h_2^* h_3 + a_4 (g_1 g_2) h_2^* h_4 + g_1 \eta_1 h_2^*\right) -$$
$$\left(-a_2 |h_1|^2 + a_1 h_1 h_2^* - a_4 (g_1 g_2)^* h_1 h_3^* + a_3 (g_1 g_2)^* h_1 h_4^* + g_1^* \eta_2^* h_1\right)$$

$$= \left(a_2 |h_1|^2 + a_2 |h_2|^2 + a_3 (g_1 g_2) h_2^* h_3 + a_4 (g_1 g_2) h_2^* h_4 + g_1 \eta_1 h_2^*\right) +$$
$$\left(a_4 (g_1 g_2)^* h_1 h_3^* - a_3 (g_1 g_2)^* h_1 h_4^* - g_1^* \eta_2^* h_1\right)$$

$$= \underbrace{\left(|h_1|^2 + |h_2|^2\right) a_2}_{S} + \underbrace{a_3 (g_1 g_2) h_2^* h_3 - a_3 (g_1 g_2)^* h_1 h_4^* + g_1 \eta_1 h_2^*}_{N_1} +$$
$$\underbrace{\left(+ a_4 (g_1 g_2) h_2^* h_4 + a_4 (g_1 g_2)^* h_1 h_3^* - g_1^* \eta_2^* h_1\right)}_{N_2} \qquad (5.53)$$

By using the same method in obtaining *Equations (5.52)* and *(5.53)*, Equations *(5.38c)* to *(5.38h)* are substituted into *Equations (5.23)* to *(5.28)*, to yield:

$$\Delta_1^2 h_3^* + (\Delta_2^2)^* h_4 = \underbrace{\left(|h_3|^2 + |h_4|^2\right) a_3}_{S} + \underbrace{a_1 (g_1 g_2) h_1 h_3^* + a_1 (g_1 g_2)^* h_2^* h_4 + g_2 \eta_1 h_3^* +}_{N_1}$$
$$\underbrace{\left(a_2 (g_1 g_2) h_2 h_3^* - a_2 (g_1 g_2)^* h_1^* h_4 + g_2^* \eta_2^* h_4\right)}_{N_2} \qquad (5.54)$$

and

$$\Delta_1^2 h_4^* - (\Delta_2^2)^* h_3 = \underbrace{\left(|h_3|^2 + |h_4|^2\right) a_4}_{S} + \underbrace{a_1 (g_1 g_2) h_1 h_4^* - a_1 (g_1 g_2)^* h_2^* h_3 + g_2 \eta_1 h_4^*}_{N_1} +$$

$$\underbrace{\left(+a_2(g_1g_2)h_2h_4^* + a_2(g_1g_2)^* h_1^* h_3 - g_2^*\eta_2^* h_3\right)}_{N_2} \tag{5.55}$$

is obtained from substituting *Equations (5.38e)* and *(5.38f)* into *Equations (5.23)* and *(5.24)*. Also note that *Equations (5.52)* to *(5.55)* are symbols detected over $t = 1$ and $t = 2$.

At $t = 3$ and $t = 4$, *Equations (5.56)* and *(5.57)* are obtained by substituting *Equation (5.38g)* and *(5.38h)* into *Equation (5.25)* and *(5.26)*

$$\Delta_3^1 h_1^* + (\Delta_4^1)^* h_2 = \underbrace{\left(|h_1|^2 + |h_2|^2\right)a_3}_{S} + \underbrace{a_1(g_1g_2)h_1^* h_3 + a_1(g_1g_2)^* h_2 h_4^* + g_1\eta_3 h_1^* +}_{N_1}$$
$$\underbrace{\left(a_2(g_1g_2)h_1^* h_4 - a_2(g_1g_2)^* h_2 h_3^* + g_1^*\eta_4^* h_2\right)}_{N_2} \tag{5.56}$$

and

$$\Delta_3^1 h_2^* - (\Delta_4^1)^* h_1 = \underbrace{\left(|h_1|^2 + |h_2|^2\right)a_4}_{S} + \underbrace{a_1(g_1g_2)h_2^* h_3 - a_1(g_1g_2)^* h_1 h_4^* + g_1\eta_3 h_2^* +}_{N_1}$$
$$\underbrace{\left(+a_2(g_1g_2)h_2^* h_4 + a_2(g_1g_2)^* h_1 h_3^* - g_1^*\eta_4^* h_1\right)}_{N_2} \tag{5.57}$$

and *Equations (5.58)* and *(5.59)* are obtained by substituting *Equations (5.38e)* and *(5.38f)* into *Equations (5.27)* and *(5.28)*

$$\Delta_3^2 h_3^* + (\Delta_4^2)^* h_4 = \underbrace{\left(|h_3|^2 + |h_4|^2\right)a_1}_{S} + \underbrace{a_3(g_1g_2)h_1 h_3^* + a_3(g_1g_2)^* h_2^* h_4 + g_2\eta_3 h_3^* +}_{N_1}$$
$$\underbrace{\left(a_4(g_1g_2)h_2 h_3^* - a_4(g_1g_2)^* h_1^* h_4 + g_2^*\eta_4^* h_4\right)}_{N_2} \tag{5.58}$$

and

$$\Delta_3^2 h_4^* - (\Delta_4^2)^* h_3 = \underbrace{\left(|h_3|^2 + |h_4|^2\right)a_2}_{S} + \underbrace{a_3(g_1g_2)h_1 h_4^* - a_3(g_1g_2)^* h_2^* h_3 + g_2\eta_3 h_4^* +}_{N_1}$$
$$\underbrace{\left(+a_4(g_1g_2)h_2 h_4^* + a_4(g_1g_2)^* h_1^* h_3 - g_2^*\eta_4^* h_3\right)}_{N_2} \tag{5.59}$$

Using *Equation (5.7)* all of the Equations of similar symbols are added, i.e. *Equations (5.52)* and *(5.58)* for symbol b_1, *Equations (5.53)* and *(5.59)* for symbol b_2, *Equations (5.54)* and *(5.56)* for symbol b_3, and *Equations (5.55)* and *(5.57)* for symbol b_4.

$$\hat{a}_1 = \underbrace{\left(|h_1|^2 + |h_2|^2 + |h_3|^2 + |h_4|^2\right)a_1}_{S} + \underbrace{a_3(g_1g_2)h_1^*h_3 + a_3(g_1g_2)^*h_2h_4^* + g_1\eta_1h_1^* + g_1^*\eta_2^*h_2 +}_{N_1}$$

$$\underbrace{a_3(g_1g_2)h_1h_3^* + a_3(g_1g_2)^*h_2^*h_4 + g_2\eta_3h_3^* + g_2^*\eta_4^*h_4}_{N_2} \quad (5.60)$$

$$\hat{a}_2 = \underbrace{\left(|h_1|^2 + |h_2|^2 + |h_3|^2 + |h_4|^2\right)a_2}_{S} + \underbrace{a_4(g_1g_2)h_2^*h_4 + a_4(g_1g_2)^*h_1h_3^* - g_1^*\eta_2^*h_1 + g_1\eta_1h_2^* +}_{N_1}$$

$$\underbrace{a_4(g_1g_2)h_2h_4^* + a_4(g_1g_2)^*h_1^*h_3 - g_2^*\eta_4^*h_3 + g_2\eta_3h_4^*}_{N_2} \quad (5.61)$$

$$\hat{a}_3 = \underbrace{\left(|h_1|^2 + |h_2|^2 + |h_3|^2 + |h_4|^2\right)a_3}_{S} + \underbrace{a_1(g_1g_2)h_1h_3^* + a_1(g_1g_2)^*h_2^*h_4 + g_2\eta_1h_3^* + g_2^*\eta_2^*h_4}_{N_1}$$

$$\underbrace{a_1(g_1g_2)h_1^*h_3 + a_1(g_1g_2)^*h_2h_4^* + g_1\eta_3h_1^* + g_1^*\eta_4^*h_2}_{N_2} \quad (5.62)$$

$$\hat{a}_4 = \underbrace{\left(|h_1|^2 + |h_2|^2 + |h_3|^2 + |h_4|^2\right)a_4}_{S} + \underbrace{a_2(g_1g_2)h_2h_4^* + a_2(g_1g_2)^*h_1^*h_3 - g_2^*\eta_2^*h_3 + g_2\eta_1h_4^* +}_{N_1}$$

$$\underbrace{a_2(g_1g_2)h_2^*h_4 + a_2(g_1g_2)^*h_1h_3^* - g_1^*\eta_4^*h_1 + g_1\eta_3h_2^*}_{N_2} \quad (5.63)$$

Comparing *Equations (5.60)* to *(5.63)* with *Equations (5.48)* to *(5.51)*, it can be seen that up to 4 times as much self noise is created in the DSSTS scheme when non-perfect cross-correlation occurs.

5.2 DSSTS CAPACITY

As mentioned earlier in this dissertation, the DSSTS is a transmit diversity scheme. In most cases with transmit diversity, the transmitter does not have knowledge of the channel. Hence,

the open-loop capacity for a Multiple-Input Single-Output (MISO) system with n transmit antennas applies [27]

$$CAP_{n,1}^{MISO,\max} = \log_2\left(1+\frac{SNR}{n}\sum_{i=1}^{n}|h_i|^2\right) \tag{5.64}$$

where h_i is the gain for receive antenna i and the normalisation by n ensures a fixed total transmitter power. Note that *Equation (5.64)* is obtained by substituting in *Chapter 2, Section 2.5, Equation (2.32)*, $m = 1$ and $H = \begin{bmatrix} h_1 & h_2 \cdots h_n \end{bmatrix}$.

The channel capacity of the DSSTS scheme can best be described by means of an example. By using the example of *Section 5.1.2*, *Equation (5.10)*, the transmission matrix of the DSSTS scheme, employing four transmit antennas, can be written as

$$T_4 = \begin{bmatrix} g_1x_1 & g_1x_2 & g_2x_3 & g_2x_4 \\ -g_1x_2^* & g_1x_1^* & -g_2x_4^* & g_2x_3^* \\ g_1x_3 & g_1x_4 & g_2x_1 & g_2x_2 \\ -g_1x_4^* & g_1x_3^* & -g_2x_2^* & g_2x_1^* \end{bmatrix} \tag{5.65}$$

Thus, form *Chapter 2, Section 2.5, Equation (2.27)*, received signal can written as

$$\bar{r} = T_4\bar{h} + \bar{\eta} \tag{5.66}$$

where $\bar{h} = \begin{bmatrix} h_1 & h_2 & h_3 & h_4 \end{bmatrix}^T$ and $\bar{\eta} = \begin{bmatrix} \eta_1 & \eta_2 & \eta_3 & \eta_4 \end{bmatrix}^T$

Thus, the four baseband signals arriving at the receive antenna can be expressed as

$$\begin{bmatrix} r_1 \\ r_2 \\ r_3 \\ r_4 \end{bmatrix} = \begin{bmatrix} g_1x_1h_1 + g_1x_2h_2 + g_2x_3h_3 + g_2x_4h_4 \\ -g_1x_2^*h_1 + g_1x_1^*h_2 - g_2x_4^*h_3 + g_2x_3^*h_4 \\ g_1x_3h_1 + g_1x_4h_2 + g_2x_1h_3 + g_2x_2h_4 \\ -g_1x_4^*h_1 + g_1x_3^*h_2 - g_2x_2^*h_3 + g_2x_1^*h_4 \end{bmatrix} + \begin{bmatrix} \eta_1 \\ \eta_2 \\ \eta_3 \\ \eta_4 \end{bmatrix} \tag{5.67}$$

By conjugating the second and fourth received signals, *Equation (5.67)* can equivalently be rewritten as

$$\begin{bmatrix} r_1 \\ r_2^* \\ r_3 \\ r_4^* \end{bmatrix} = \begin{bmatrix} g_1h_1 & g_1h_2 & g_2h_3 & g_2h_4 \\ g_1^*h_2^* & -g_1^*h_1^* & g_2h_4^* & -g_2^*h_3^* \\ g_2h_3 & g_2h_4 & g_1h_1 & g_1h_2 \\ g_2h_4^* & -g_2h_3^* & g_1h_2^* & -g_1h_1^* \end{bmatrix} \begin{bmatrix} x_1 \\ x_2 \\ x_3 \\ x_4 \end{bmatrix} + \begin{bmatrix} \eta_1 \\ \eta_2^* \\ \eta_3 \\ \eta_4^* \end{bmatrix} \tag{5.68}$$

Note that the condition stated in *Chapter 2, Section 2.5, Equation (2.30)* is satisfied by *Equation (5.68)*. After matched-filtering with H, we obtain

$$\begin{aligned} \hat{\bar{r}} &= H^H \bar{r} \\ &= \begin{bmatrix} |h_1|^2+|h_2|^2+|h_3|^2+|h_4|^2 & 0 & \cdots \\ 0 & |h_1|^2+|h_2|^2+|h_3|^2+|h_4|^2 & \\ 0 & 0 & \cdots \\ 0 & 0 & \end{bmatrix} \\ &\quad \begin{bmatrix} 0 & 0 \\ 0 & 0 \\ |h_1|^2+|h_2|^2+|h_3|^2+|h_4|^2 & 0 \\ 0 & |h_1|^2+|h_2|^2+|h_3|^2+|h_4|^2 \end{bmatrix} \begin{bmatrix} x_1 \\ x_2 \\ x_3 \\ x_4 \end{bmatrix} + \begin{bmatrix} \eta_1 \\ \eta_2^* \\ \eta_3 \\ \eta_4^* \end{bmatrix} \end{aligned} \tag{5.69}$$

where the noise vector $\bar{\eta}$ remains white. Note that the DSSTS scheme is fully decomposable in four (1,1) systems, where each has ¼ of the transmitted power. Thus, the total capacity of the DSSTS scheme with four transmit antennas is

$$CAP_{4,1}^{DSSTS} = \log_2\left(1+\frac{SNR}{4}\left(|h_1|^2+|h_2|^2+|h_3|^2+|h_4|^2\right)\right) \tag{5.70}$$

Comparing *Equation (5.70)* to *Equation (5.64)*, we see that

$$CAP_{4,1}^{DSSTS} = CAP_{4,1}^{MISO,\max} \tag{5.71}$$

Following the same reasoning for obtaining *Equation (5.71)*, similar results may be derived for the DSSTS 6, 8 and 10 transmit antenna scenarios. In general, the capacity performance of the DSSTS is similar to the open-loop capacity given in *Equation (5.72)*

$$CAP_{n,1}^{DSSTS} = CAP_{n,1}^{MISO,\max} \tag{5.72}$$

Capacity plots for the DSSTS with 2, 4, 6 transmit antennas, that is equal to $CAP_{n,1}^{MISO,\max}$, are plotted in *Chapter 6, Figure 6.23*. Note that the capacity increases as the number of transmit antennas increases. Also note that Capacity plots of other transmit diversity schemes, i.e. the Zero Forcing (ZF) [18] and a proposed (4x1) transmit diversity scheme in [18] are presented in *Chapter 6, Figure 6.23*. These are included to show the relative performance of the DSSTS schemes considered.

5.3 DSSTS PERFORMANCE EVALUTION PLATFORM

The complete FFCS platform used in this dissertation is shown in *Figure 5.4,* and the configuration parameters are presented in *Table 5.1*. This platform is built around the DSSTS scheme's encoder and decoder structures, discussed in *Sections 5.1.2* and 5*.1.3*.

At any given time, the bitstream $\bar{b}$ arrives at the DSSTS encoder (see *Section 5.1.1*). This bitstream is encoded and transmitted from antennas 1 to *n*. By using a complex FFCS from *Chapter 4, Section 4.1*, each symbol transmitted from an antenna is separated into it's real, $\mathrm{Re}\{\bullet\}$ and Imaginary, $\mathrm{Im}\{\bullet\}$ parts. At the receiver side, all the real and imaginary parts are added respectively. AWGN, denoted as η, and described in Appendix C*, Section C.5*, is added to the real and imaginary parts respectively and decoded by the DSSTS scheme's decoder. The decoder uses perfect CSI, denoted by *h*, from all the different channels used in the simulation, in order to decode the received bitstream. The output bitstream $\hat{\bar{b}}$ from the decoder is compared to the input bitstream $\bar{b}$ and the BER is calculated. These BER graphs are presented and discussed in *Chapter 6*.

Configuration Parameter	Setting
Unspread Symbol Rate	1000 [symbols/s]
Spreading Sequence Length, *N*	32 [chips]
Spreading Sequence Rate	32000 [chips/s]
Effective RF Carrier Frequency	900 [MHz]
Receiver Configuration	ML detection
Symbol Synchronization	Perfect
Carrier Synchronization	Perfect
Code Lock	Perfect
Spreading Sequences Supported	Walsh

Table 5.1. DSSTS Simulation Configurations.

Up to 10 transmit antennas are used in this simulation study, depicted in *Figure 5.4*. For each of the 10 transmit antennas, a complex FFCS, based on independent *Clarke*-based complex FFCS, were used to realise the 10 distinct transmission paths transversed by the outputs of the DSSTS scheme. The channels are also assumed to be quasi-static over two consecutive time periods in order to decode the received symbols by means of the ST decoder (see *Section 5.1.3*) In other words, every second time interval the channels experience statistical independent fading. Although this seems very unrealistic in a real world scenario, this method had to be used in order to compare it to the original Alamouti scheme's performance presented in [2].

Perfect power control was assumed, i.e. the average powers of all the users' corrupted signals received at the receive antenna are equal. As described in *Chapter 4*, the complex FFCS can be set to Doppler frequencies of 33, 66, and 100Hz to simulate spectral broadening due to mobility (i.e. fast fading), and the Rician factor determines the ratio of the LOS to NLOS components in the channel simulator. If *K*, in a dB scale, is large, the LOS is more prominent and Rician fading occurs. On the other hand if $K \to -\infty$ dB, the NLOS factor is more prominent and Rayleigh fading occurs. Perfect carrier, chip and symbol synchronisation were assumed at the receiver over the entire frame length *l* and perfect CSI was used by the decoder to decode the received symbols.

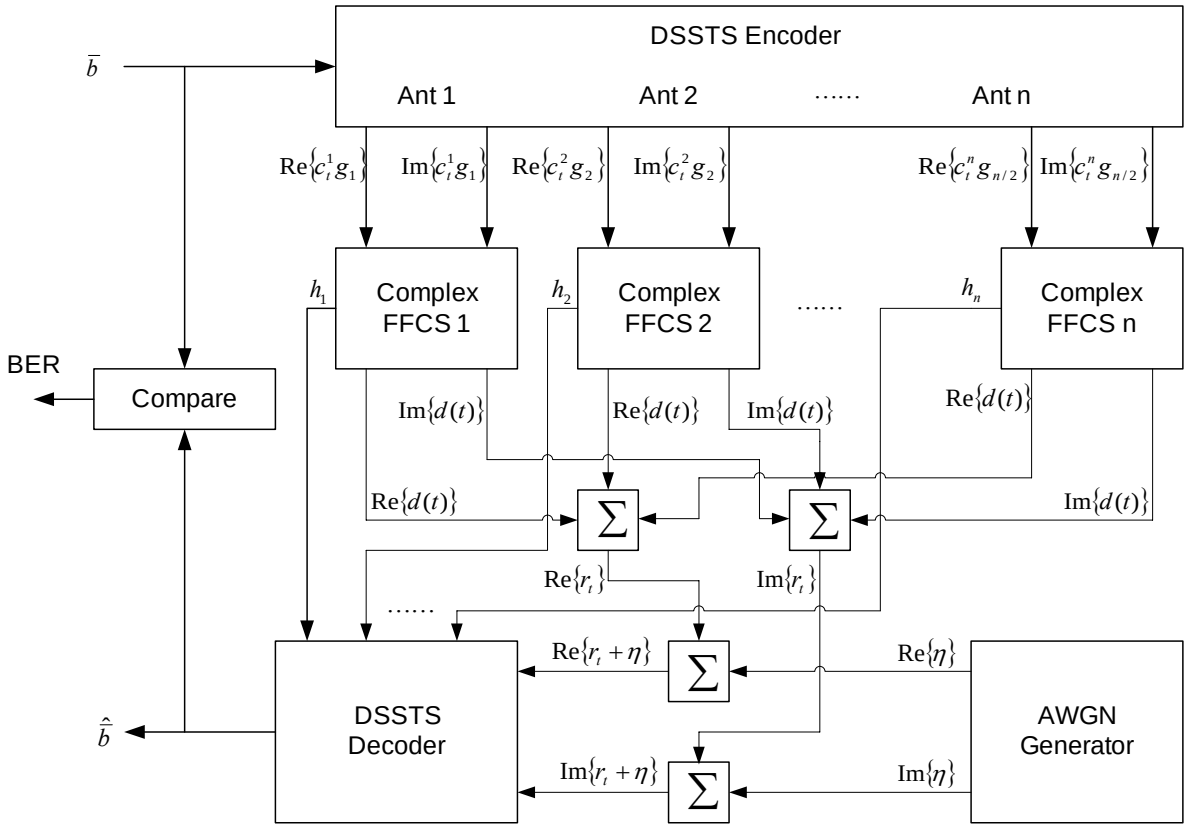

Figure 5.4. Performance evaluation platform of the new DSSTS scheme.

5.4 A SPACE - SEQUENCE TRANSMIT DIVERSITY SCHEME: SSTD

In *Chapter 3*, it was stated that Alamouti's classic ST coding scheme has an unrealistic assumption in the decoupling stage for environments with a low throughput rate and high Doppler component, i.e. that the channel is quasi-static over two consecutive symbol intervals. To address this deficiency, a new scheme called, Space-Sequence Transmit Diversity (SSTD), has been proposed by Maasdorp *et al*. [19, 20]. The proposed SSTD scheme is in essence a combination between the Alamouti matrix and a DS/SSMA scheme using CSSs, facilitating the transmission of all the ST symbols in one time interval. Also note that only a general overview of the SSTD is presented here in order to show that the quasi-static channel assumption can be addressed. Background information on CSSs, as well as detailed descriptions of the complex DS/SSMA QPSK transmitter and RAKE receiver simulator structures, can be obtained from Maasdorp *et al*. [19, 20].

5.4.1 SSTD encoder structure

Figure 5.5 shows the proposed SSTD encoder structure, constructed using four complex DS/SSMA QPSK transmitters. This diversity encoder is based on *Alamouti*'s original STC scheme, described in *Chapter 2*, *Section 2.2.2*. It functions as follows:

At the *m'th* encoding instance, four consecutive antipodal input data bits are inserted into the vector $b_m^q = \left[b_{m,0}^q \quad b_{m,1}^q \quad b_{m,2}^q \quad b_{m,3}^q \right]$. Using the following mapping, this vector is encoded into a 2-bit complex input (represented by the respective I-channel and Q-channel bits, $c_m^{I,(q,z)}$ and $c_m^{Q,(q,z)}$, with z = 0; 1; 2; 3) for each of the four complex DS/SSMA QPSK transmitters in user-q's SSTD encoder:

$$\begin{bmatrix} c_m^{I,(q,0)} = c_m^{I,(q,3)} \\ c_m^{I,(q,0)} = -c_m^{I,(q,3)} \\ c_m^{I,(q,1)} = -c_m^{I,(q,3)} \\ c_m^{I,(q,1)} = c_m^{I,(q,3)} \end{bmatrix} = \begin{bmatrix} 1 & 0 & 0 & 0 \\ 0 & 1 & 0 & 0 \\ 0 & 0 & -1 & 0 \\ 0 & 0 & 0 & 1 \end{bmatrix} \begin{bmatrix} b_{m,0}^q \\ b_{m,1}^q \\ b_{m,2}^q \\ b_{m,3}^q \end{bmatrix} \tag{5.73}$$

Thus, the wideband transmitters in the SSTD encoder (described in Maasdorp *et al*. [19]) each transmit W = 1 complex symbols during the m'th encoding instance. Let $\Omega_m^{(q,z)}(t)$, with z = 0; 1; 2; 3, denote the output waveforms generated by the 4 transmitters in user-q's SSTD encoder. These output waveforms, representing complex transmitter output symbols from the alphabet $\nu = \{\nu_0 \quad \nu_1 \quad \nu_2 \quad \nu_3\}$ (see *Equation (5.78)*), are now transmitted on the antenna pair, y=1 and y=2, using the following transmission matrix:

$$T = \begin{bmatrix} \Omega_m^{(q,0)}(t) & \Omega_m^{(q,2)}(t) \\ \Omega_m^{(q,1)}(t) & \Omega_m^{(q,3)}(t) \end{bmatrix} \begin{matrix} \} \\ \} \end{matrix} \begin{matrix} Transmits\ during \\ I_0 \end{matrix}$$
$$\begin{matrix} \uparrow & \uparrow \\ y=1 & y=2 \end{matrix} \tag{5.74}$$

where $I_0 : m \cdot T_s < t \le (m+1) \cdot T_s$ Thus, the outputs emanating from antenna y=1 and y=2 are given by:

$$s_m^{y=1,q}(t) = \mathrm{Re}\left\{\Omega_m^{(q,0)}(t)\right\} + \mathrm{Re}\left\{\Omega_m^{(q,1)}(t)\right\} + j\left(\mathrm{Im}\left\{\Omega_m^{(q,0)}(t)\right\} + \mathrm{Im}\left\{\Omega_m^{(q,1)}(t)\right\}\right) \qquad (5.75)$$

$$s_m^{y=2,q}(t) = \mathrm{Re}\left\{\Omega_m^{(q,2)}(t)\right\} + \mathrm{Re}\left\{\Omega_m^{(q,3)}(t)\right\} + j\left(\mathrm{Im}\left\{\Omega_m^{(q,2)}(t)\right\} + \mathrm{Im}\left\{\Omega_m^{(q,3)}(t)\right\}\right) \qquad (5.76)$$

respectively. Note that the assignment of CSSs to the 4 wideband complex DS/SSMA QPSK transmitters, to form a single user's SSTD encoder, constitutes a major design challenge.

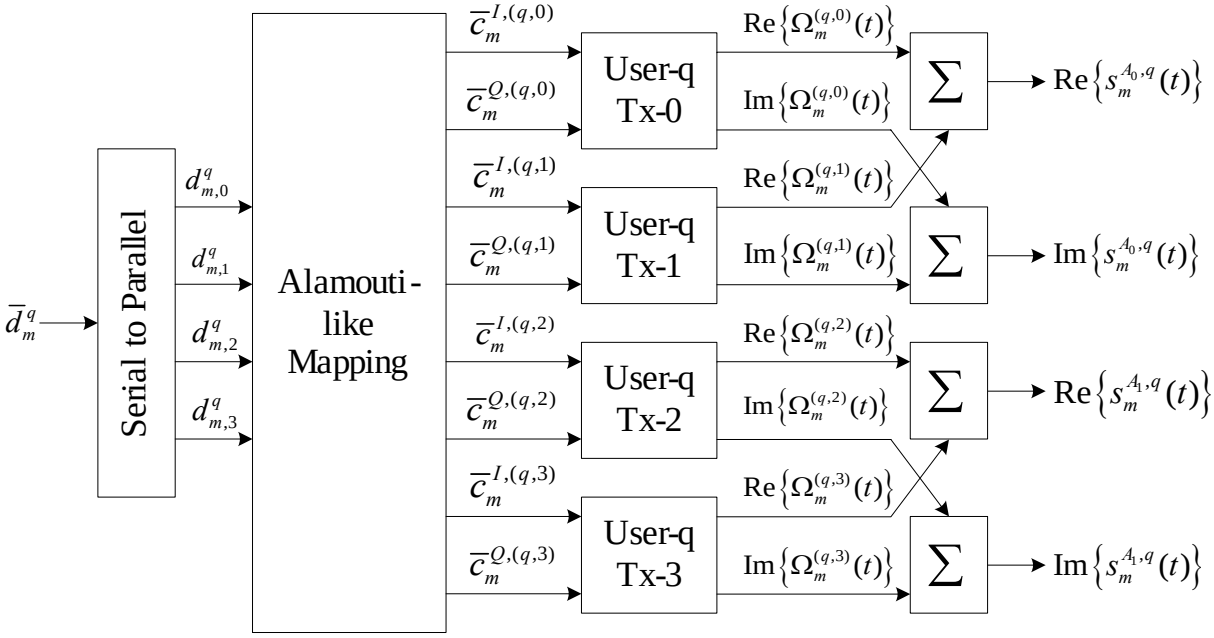

Figure 5.5. Proposed SSTD Encoder for user-q.

Presently, only two possible CSS assignment options were evaluated in this particular study, as described in *Chapter 6, section 6.4*. Also note that the transmit matrix *T* in *Equation (5.74)* is transmitted in one symbol time interval, as described by *Equations (5.75)* and *(5.76)*. Thus forcing the two consecutive symbols transmitted from antennas y=1 and y=2 respectively to have the same fading as they propagate through a channel path as a combined symbol. This effectively means that the assumption of the channel having to be quasi-static can be neglected, but the same decoding algorithm can be used.

5.4.2 SSTD decoder structure

Figure 5.6 shows the proposed SSTD decoder structure, constructed using four complex DS/SSMA QPSK RAKE receivers. The decoding process firstly involves demodulation of the received signals $r_m^{(q,k)}(t) = r_m^q(t)$ using the four separate RAKE receivers to obtain $y_m^{(q,k)}$, for k = 0, 1, 2, 3. These soft outputs are then appropriately combined to give $\overline{u}_m^{0,q}$ and $\overline{u}_m^{1,q}$.

Next, the following set of Euclidian distance metrics must be calculated for all combinations of the index parameters i = 0, 1, 2, 3 and j = 0, 1, 2, 3:

$$DM_{i,j}^{q} = \left|u_m^{0,q} - \hat{\alpha}_m^{n=1,q} \cdot v_i - \hat{\alpha}_m^{n=2,q} \cdot v_j\right|^2 + \left|u_m^{1,q} + \hat{\alpha}_m^{n=1,q} \cdot v_j^* - \hat{\alpha}_m^{n=2,q} \cdot v_i^*\right|^2 \qquad (5.77)$$

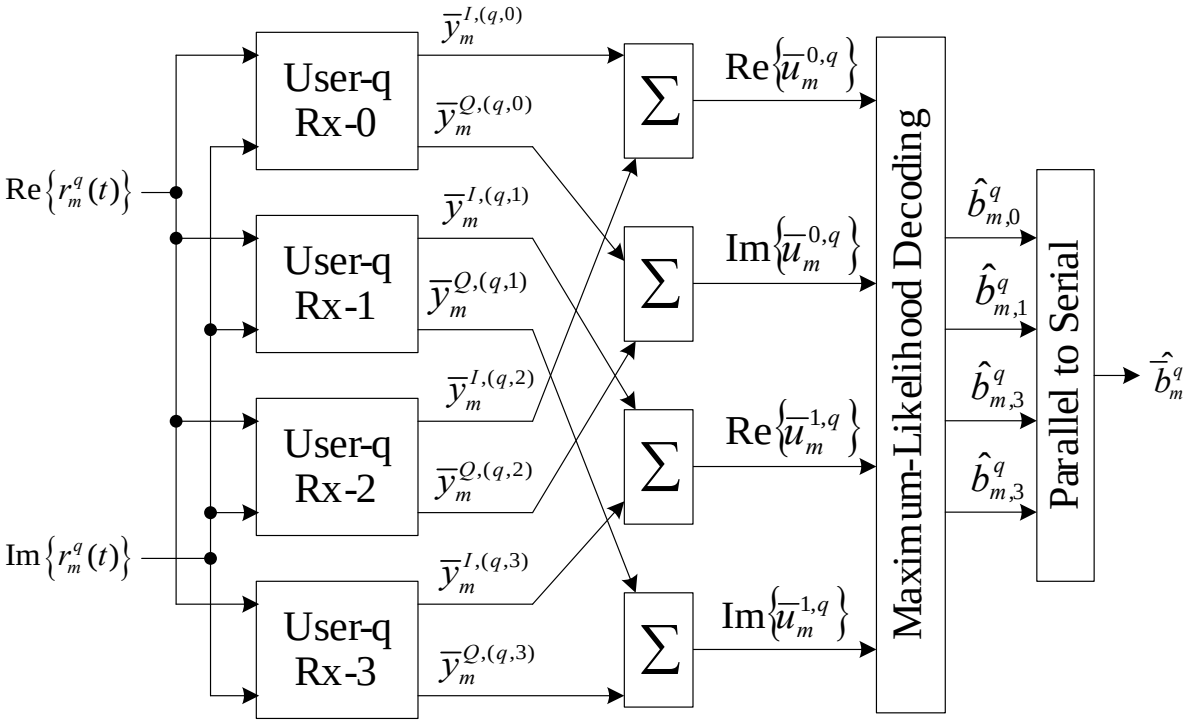

Figure 5.6. Proposed SSTD Decoder for user-q.

where $\nu_i \in \nu$ and $\nu_j \in \nu$, with ν the set of possible complex DS/SSMA QPSK output symbols, defined as follows:

$$\begin{aligned}\nu &= \{\nu_0 \quad \nu_1 \quad \nu_2 \quad \nu_3\} \\ &= \{(1, i) \quad (1,-i) \quad (-1,-i) \quad (-1, i)\}\end{aligned} \tag{5.78}$$

The average fading amplitude estimates associated with the signals transmitted by antenna y=1 and y=2 are given by $\hat{\alpha}_m^{n=1,q} = \hat{\alpha}_m^{(q,0)} = \hat{\alpha}_m^{(q,1)}$ and $\hat{\alpha}_m^{n=2,q} = \hat{\alpha}_m^{(q,2)} = \hat{\alpha}_m^{(q,3)}$ respectively. Maximum-Likelihood (ML) decoding involves finding $\min\{DM_{i,j}^q\} = DM_{i\,ML,j\,ML}^q$ over all combinations of i and j. The SSTD decoder's four output bit estimates are then determined as follows: $\hat{b}_{m,0}^q = \mathrm{Re}\{\nu_{i\,ML}\}, \hat{b}_{m,1}^q = \mathrm{Im}\{\nu_{i\,ML}\}, \hat{b}_{m,2}^q = \mathrm{Re}\{\nu_{jML}\}$ and $\hat{b}_{m,3}^q = \mathrm{Im}\{\nu_{j\,ML}\}$.